SYNTHESIS, CHARACTERIZATION, AND POLYMERIZATION OF POLYETHER BRIDGED THIOPHENE AND ANILINE DERIVATIVES

A THESIS SUBMITTED TO
THE GRADUATE SCHOOL OF NATURAL AND APPLIED SCIENCES
OF
MIDDLE EAST TECHNICAL UNIVERSITY

BY

SEHA TİRKEŞ

IN PARTIAL FULFILLMENT OF THE REQUIREMENTS
FOR
THE DEGREE OF DOCTOR OF PHILOSOPHY
IN
POLYMER SCIENCE AND TECHNOLOGY

FEBRUARY 2008

Approval of the thesis:

SYNTHESIS, CHARACTERIZATION, AND POLYMERIZATION OF POLYETHER BRIDGED THIOPHENE AND ANILINE DERIVATIVES

submitted by **SEHA TİRKEŞ** in partial fulfillment of the requirements for the degree of **Doctor of Philosophy in Polymer Science and Technology Department, Middle East Technical University** by,

Prof. Dr. Canan Özgen
Dean, Graduate School of **Natural and Applied Sciences**

Assoc. Prof. Dr. Göknur Bayram
Head of Department, **Polymer Science and Technology**

Prof. Dr. Ahmet M. Önal
Supervisor, **Chemistry Department, METU**

Examining Committee Members:

Prof. Dr. Zuhal Küçükyavuz
Chemistry Dept., METU

Prof. Dr. Ahmet M. Önal
Chemistry Dept., METU

Assoc. Prof. Dr. Göknur Bayram
Chemical Engineering Dept., METU

Prof. Dr. Levent K. Toppare
Chemistry Dept., METU

Prof. Dr. Kadir Pekmez
Chemistry Dept., Hacettepe University

Date: February 22, 2008

I hereby declare that all information in this document has been obtained and presented in accordance with academic rules and ethical conduct. I also declare that, as required by these rules and conduct, I have fully cited and referenced all material and results that are not original to this work.

Name, Last Name : Seha Tirkeş

Signature :

ABSTRACT

SYNTHESIS, CHARACTERIZATION AND POLYMERIZATION OF POLYETHER BRIDGED THIOPHENE AND ANILINE DERIVATIVES S

Tirkeş, Seha
Ph. D., Department of Polymer Science and Technology
Supervisor: Prof. Dr. Ahmet M. Önal

February 2008, 86 Pages

New compounds consisting of 3-thienyl and aniline units linked by polyether bridges have been synthesized and their electrochemical polymerization was performed via constant potential electrolysis and cyclic voltammetry. In the case of 3-thienyl derivatives two compounds, 1,12-di-3-thienyl-2,5,8,11-tetraoxadodecane (**MI**) and 1,15-di-3-thienyl-2,5,8,11,14-pentaoxapentadecane (**MII**) were synthesized utilizing literature methods and their corresponding polymers, poly(**I**) and poly(**II**) were prepared in an electrolytic solution containing 0.1 M terabutylammonium hexafluorophosphate (TBAPF6) dissolved in CH_3CN. On the other hand, polymerization of aniline derivatives, 2,2'-[ethane-1,2-diylbis(oxyethane-2,1-diyloxy)]dianiline (**MIII**) and 2,2'-[oxybis(ethane-2,1-diyloxyethane-2,1-diyloxy)]dianiline (**MIV**), was achieved in an aqueous solution containing 3.0 mol.L^{-1} H_2SO_4. Spectroelectrochemical (SPEL) properties and thermal analysis of the resulting polymers have been investigated using UV-vis, and Thermogravimetric Analysis (TGA). **MIII** was also polymerized via chemical oxidation for comparison purposes. The polymers were characterized using ^1H-NMR and FT-IR spectroscopic techniques. Furthermore, copolymers of **MIII** and

MIV with aniline (ANI) were also studied with cyclic voltammetry (CV). SPEL behavior and electrical conduction mechanism of resulting copolymers were investigated using UV-vis spectroscopic technique and four-point probe technique, respectively.

Keywords: Electrochemical Polymerization, SPEL Properties, Polyether Bridged Substituted Thiophenes, Polyether Bridged Substituted Anilines

ÖZ

POLİETER KÖPRÜLÜ TİYOFEN VE ANİLİN TÜREVLERİNİN SENTEZİ, KAREKTERİZASYONU POLİMERİZASYONU

Tirkeş, Seha
Doktora, Polimer Bilimi ve Teknolojisi Bölümü
Tez Yöneticisi: Prof. Dr. Ahmet M. Önal

Şubat 2008, 86 Sayfa

3-tiyenil ve anilin birimlerinin polieter köprüsü ile bağlanmış yeni bileşikleri sentezlendi ve bunların elektrokimyasal polimerizasyonu sabit potansiyel ve dönüşümlü voltametri teknikleri kullanılarak gerçekleştirildi. 3-tiyenil türevleri; 1,12-di-3-tiyenil-2,5,8,11-tetraokzadodekan (**MI**) ve 1,15-di-3-tiyenil-2,5,8,11,14-pentaokzapentadekan (**MII**) literatürdeki mevcut yöntemler kullanılarak hazırlandı ve bu monomerlerin polimerleri, poli(**I**) ve poli(**II**), 0.1 M tetrabütilamonyum hekzafulorofosfat (TBABF6) içeren CH_3CN çözeltisi içinde sentezlendi. Diğer yandan, anilin türevlerinin, 2,2'-[etan-1,2-diyilbis(oksietan-2,1-diyiloksi)]dianilin (**MIII**) ve 2,2'-[oksibis(etan-2,1-diyiloksietan-2,1-diyiloksi)]dianilin (**MIV**), polimerleri 3.0 $mol.L^{-1}$ s H_2SO_4 sulu çözeltisinde sentezlendi. Spektroelektrokimyasal (SPEL) ve termal davranımları UV-vis ve Termogravimetrik Analiz (TGA) spektrometrik yöntemleri ile incelendi. **MIII** monomeri karşılaştırma amacı ile ayrıca kimyasal olarak polimerleştirildi. Polimerler ^{1}H-NMR ve FT-IR spectroskopik teknikler ile karakterize edildiler. Bunların yanında **MIII** ve **MIV** monomerlerinin aniline (ANI) ile kopolimer sentezi döngülü voltametri ile çalışıldı. Bu kopolimerlerin SPEL davranımları ve elektriksel iletkenlik davranımları sırasıyla UV-vis ve dört-nokta iletkenlik teknikleri ile incelendi.

Anahtar Kelimeler: Elektrokimyasal Polimerleşme, SPEL Özellikleri, Polieter Köprülü Tiyofen Türevleri, Polieter Köprülü Anilin Türevleri.

To My Parents

ACKNOWLEDGMENTS

The author wishes to express his deepest gratitude to his supervisor Prof. Dr. Ahmet M. Önal for his guidance, advice, criticism, encouragements and insight throughout the research.

The author would like to thank Asst. Prof. Dr. Atilla Cihaner and Dr. Fatih Algı for their valuable synthesis discussions.

I would like to express my eternal gratitude to my parents, Sevgi Tirkeş and Oğuz Tirkeş, and also my brother Süha Tirkeş and his family for their never-ending support and encouragement.

TABLE OF CONTENTS

CHAPTER

LIST OF TABLES

TABLES

LIST OF FIGURES

FIGURES

ABBREVIATIONS

ASV	Anodic Stripping Voltammetry
DPASV	Differential Pulse Anodic Stripping Voltammetry
CB	Conduction Band
CP	Conducting Polymer
CPE	Constant Potential Electrolysis
CE	Counter Electrode
CES	Crown Ethers
CV	Cyclic Voltammetry
DSC	Differential Scanning Calorimetry
ESR	Electron Spin Resonance
FTIR	Fourier Transform Infrared
HOMO	Highest Occupied Molecular Orbital
ITO	Indium Tin Oxide
LUMO	Lowest Unoccupied Molecular Orbital
NMR	Nuclear Magnetic Resonance
PA	Polyacetylene
PANI	Polyaniline
PPy	Polypyrrole
Pt	Platinum
PTh	Polythiophene
Py	Pyrrole
PEDOT	Poly(3,4-ethylenedioxythiophene)
Th	Thiophene
RE	Reference Electrode
SPEL	Spectroelectrochemical
SCE	Saturated Calomel Electrode
TBAPF6	Tetrabutylammonium hexafluorophosphate
TGA	Thermogravimetric Analysis
VB	Valence Band
VRH	Variable Range Hopping
WE	Working Electrode

CHAPTER 1

INTRODUCTION

1.1 Brief History of Conjugated Polymers

Near the end of the 1970's, the field of conducting polymers (CPs) aroused with the discovery of polyacetylene (PA) that can be made highly conductive by doping [1]. Subsequently, several electron-rich CPs including polypyrrole (PPy) [2,3,4], polythiophene (PTh) [5,6], poly(3,4-ethylenedioxythiophene) (PEDOT) [7,8,9], and polyfuran [10], as well as other aromatic polymers such as polycarbazole [11], polyfluorene [12], polyaniline (PANI) [13], poly(p-phenylene vinylene) [14], and poly(p-phenylene) [15] were developed and extensively investigated as alternative CPs (Figure 1.1).

The polymers of aniline (ANI), pyrrole (Py) and thiophene (Th) are aromatic systems which have higher environmental stability and structural versatility [16]. By some modifications of monomer structure, the electronic and electrochemical properties of these polymers can be altered. The recent interest in conducting polymers is due to their practical and potential applications including organic field effect transistors[17], sensors[18], light emitting diodes[19], solar cells[20] etc.

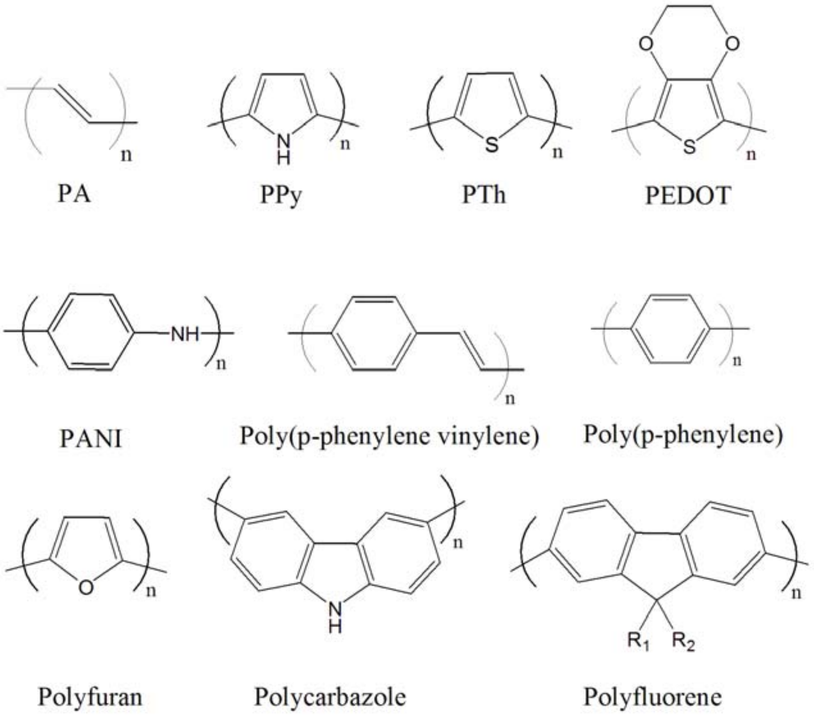

Figure 1.1 Some common conducting polymers.

1.2 Synthesis of CPs

1.2.1 Electrochemical Polymerization

In electrochemical synthesis of CPs, a suitable potential (usually the oxidation potential of monomer) is applied to the working electrode which results in the formation of reactive radical cations due to the oxidation of monomer in the electrolytic medium. There are two possible paths that follow the oxidation of monomer. The first path includes coupling of radical cation and neutral monomer, which is followed by formation of neutral dimer by loss of two protons [21,22]. On the other hand, the second path involves the coupling of two radical cations, forming a dication, followed by the loss of two protons to form neutral dimer [23,24]. Then, the neutral dimer is oxidized and the possible coupling process is repeated. The oxidation potential of dimer is lower than the monomer itself because of extended conjugation over two rings. Therefore, it is easier to oxidize the dimer to form a new radical cation. As the chain length increases, an insoluble and electroactive polymer film is deposited onto the working electrode. A proposed polymerization mechanism for heterocycles is given in Figure 1.2 (a). During the polymerization reaction, a linear and electroactive polymer chain is produced by α-α' couplings. On the other hand, possible α-β linkages cause the formation of a branched chain with more defects. Therefore α-β coupling alters the electronic properties of the polymer (Figure 1.2 (b)). This is consistent with the considerable increase in the content of disorder as well as the decrease in conductivity as the polymerization proceeds. It is known that the α and β positions have about 95/5 relative reactivity for Th and this ratio decreases as the polymerization proceeds, leading to an increase in the number of undesired couplings and consequently to a decrease in the polymer effective mean conjugation length [24].

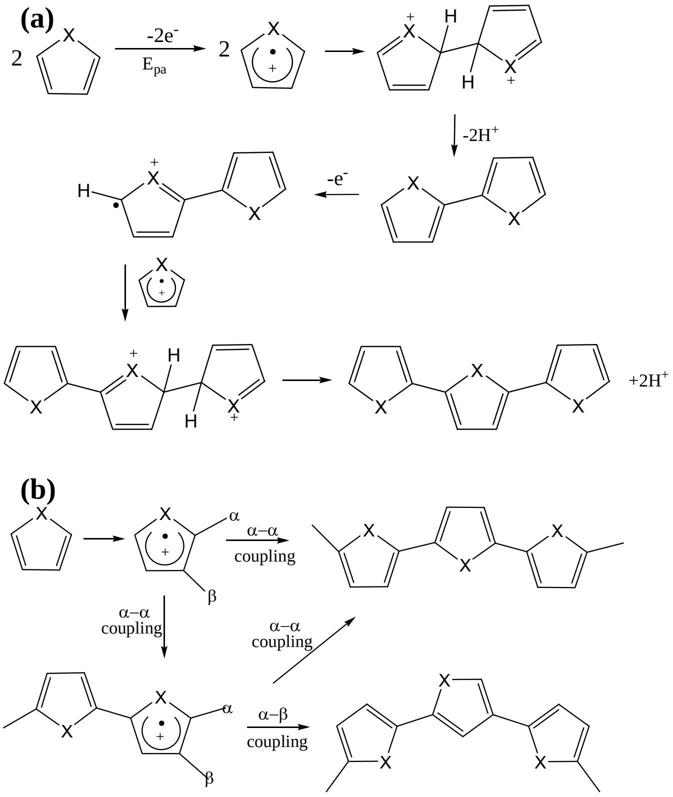

Figure 1.2 (a) Electropolymerization mechanism of heterocycles (X = S, O, NH), (b) Possible two linkage routes: α-α' and α-β linkages in unsubstituted poly(heterocycles).

The substitution of the 3- and 4- positions of such monomers with alkyl and alkoxy groups is one of the ways of eliminating undesired α-β and β-β' couplings. For example, polymerization of EDOT proceeds via desired α-α' couplings and a soluble polymer is synthesized with an enhanced degree of order due to the substitution of both –β and -β' positions.

1.2.2 Chemical Polymerization

Although electrochemical polymerization has a great number of advantages, including simplicity, this method usually leads to the formation of insoluble polymers preventing the analysis of primary structures using common techniques. Due to this drawback, chemical polymerization might be preferred in synthesizing new conductive and soluble conjugated polymers.

Chemical polymerization techniques are the least expensive and most widely exploited method to prepare conjugated polymers [25]. Instead of applying an external potential, chemical polymerization is achieved by exposing the monomer to a two-electron stoichiometric amount of oxidizing agent, resulting in the formation of the polymer in its doped and conducting state. The mechanism of chemical and electrochemical polymerizations is thought to be very similar. For example, Th and its derivatives are typically polymerized in the presence of anhydrous $FeCl_3$ [26,27], although other Lewis acids can also be used [28].

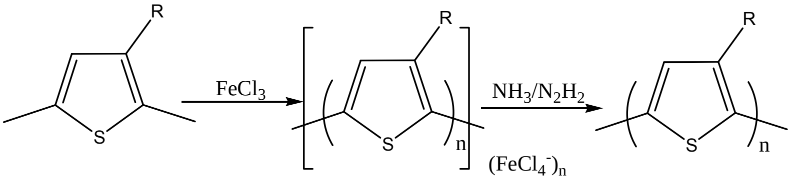

Figure 1.3 Oxidative polymerization of a substituted Th using $FeCl_3$ as a Lewis acid.

The main advantage of chemical polymerizations is that properly substituted heterocyclic and other aromatic monomers form highly soluble polymers. Therefore, the analysis and characterization of these polymers by using common characterization techniques can be realized. In addition to this, the polymerization conditions can also be modified to yield large quantities of polymer.

Although having some advantages, chemical polymerizations have several disadvantages that cause low quality polymers. The chemical polymerizations catalyzed by Lewis acid yield more rigid oxidized polymer [29] resulting in its precipitation in the polymerization medium, limiting the degree of polymerization. Also, the use of strong oxidizing agents may cause overoxidation and decomposition of the polymer and this disadvantage can be eliminated by using electrochemical methods that control the monomer oxidation potential [30,31].

1.3 Band Theory

Band theory suggests that the electrical properties of a material are the direct consequence of the energy difference (the band gap, E_g) between the lowest unoccupied molecular orbital (LUMO) and the highest occupied molecular orbital (HOMO). Metals are materials having partially or completely filled bands, where the conduction is achieved by movement of charge carriers. In semiconductors, there is a completely occupied valence band (VB) and an unoccupied conduction band (CB) separated by an E_g. The CB can be populated by exciting electrons across the band gap either thermally or photochemically. Doping of semiconductors by dopants increases the conductivity of the material depending on the degrees of doping and type of dopant (e.g. p-type or n-type) [32]. On the other hand, insulators have very large band gaps that are inaccessible under normal environmental conditions (Figure 1.4).

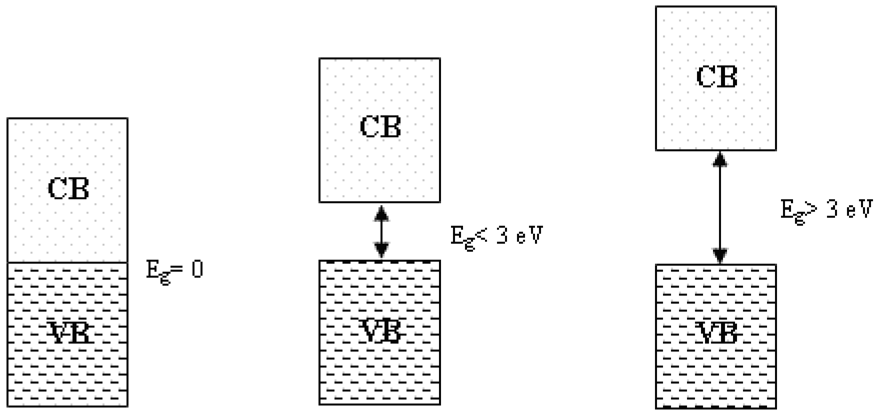

METAL SEMICONDUCTOR INSULATOR

Figure 1.4 Simple band diagrams explaining the difference among metals, semiconductors and insulators.

1.4 Doping and Conductivity of Organic Materials

The π orbital overlapping with increasing PA chain length is shown in Figure 1.5 [33,34]. Both the cis- and trans- PAs have significantly low conductivities, which were about ~10^{-13} and ~10^{-6} S/cm, respectively, in their neutral forms. Therefore, doping by adding electrons to the CB or removing electrons from the VB is essential to enhance the conductivity of PA. In the case of *cis*-PA, the ground state structure is non-degenerate and the VB is filled. Evolution of the band structure from monomer to polymer for conjugated heterocycles is similar to the one sketched in Figure 1.5.

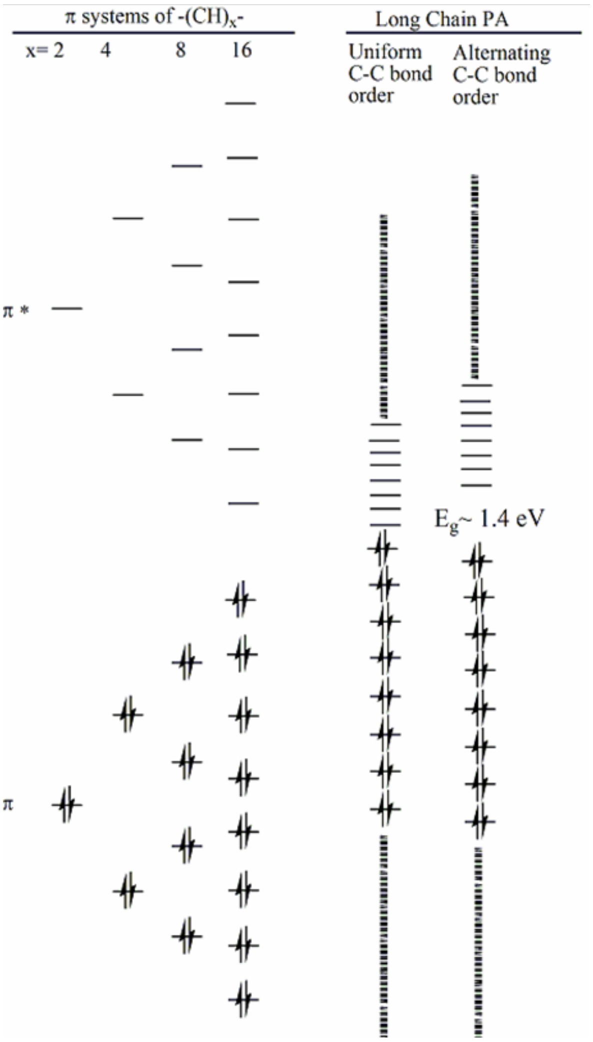

Figure 1.5 Evolution of the band gap in PA: Schematic representation of the π-molecular orbitals energy levels with increasing chain length in PA [33,34].

The unique property of PA is its degenerate ground state. Allowed optical transition from VB and CB for neutral PA, and the other transitions for neutral and charged solitons in PA are represented in Figure1.6. Neutral PA, however, has one allowed optical transition from the VB to CB as shown in Figure 1.6 (A).

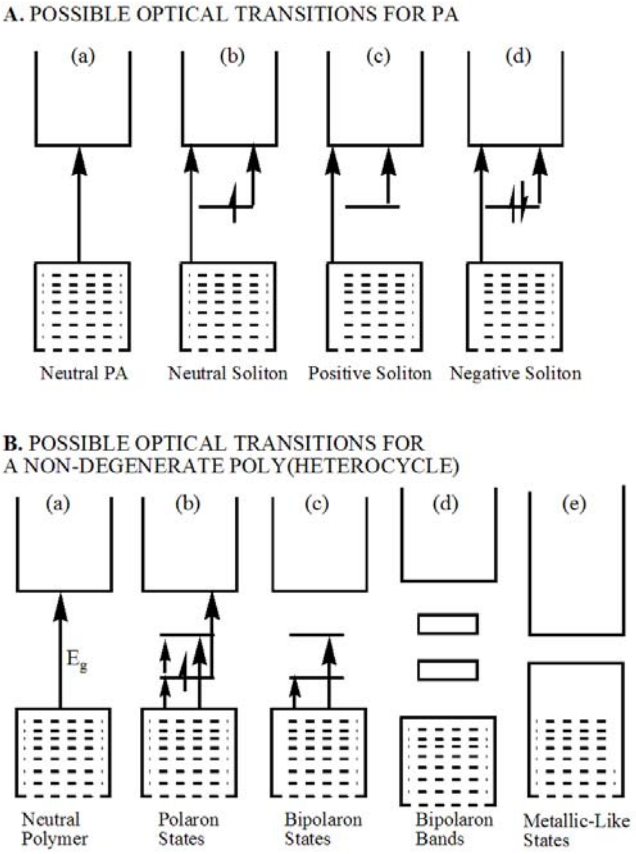

Figure 1.6 Optical transitions for doped CPs. (A) neutral PA, p-doped and n-doped PA all have a mid-gap optical transition. (B) The non degeneracy of poly(heterocycles) causes the charge carriers to be polarons or bipolarons at high doping levels.

On the contrary, the conducting polymers of poly(heterocycles) do not have degenerate states because of energy difference between the aromatic structure and quinoid structure, which has a lower ionization potential and a larger affinity than the aromatic structure [35]. This causes different optical transitions achieved by different charge carriers.

In the case of PPy, in its neutral state, it has a band gap of 3.2 eV which is in the semiconductor range (Figure 1.6 B (a)). The two polaron levels (~0.5 eV from the VB and CB) are formed by removing one electron from CP to form a polaron (see Figure 1.6 B (b)). The removal of an electron from polaron structure produces bipolaron [36], (Figure 1.6 B (c)). As it goes to very high doping level, the bipolaron states of Figure 1.6 B (c) combine to form bipolaron bands (Figure 1.6 B (d)) [37]. At these high doping levels, the spinless bipolarons achieve conductivity under the application of an electrical field. If the higher doping levels, hypothetically 100 % doping, were able to achieve, the coalescence of bipolaron levels into VB and CB would cause metal-like conduction due to the lower, half-filled valence/bipolaron band (Figure 1.6 B (e)).

Depending on the polymer type, doping can be achieved in different ways. The chemical doping by charge transfer redox chemistry was the initial way discovered at the end of the 1970s [1,38]. Exposing the polymer to the iodine vapor was the way of oxidation of polymer, and the reduction of polymer was accomplished with the treatment sodium naphthalenide (Figure 1.7 A).

A. Chemical Doping

(a) p-type doping

$(CP)_n + 3/2\ ny(I_2) \rightarrow [(CP)^{+y}(I_3^-)_y]_n$

(b) n-type doping

$(CP)_n + [Na^+(C_{10}H_8)^-]_y \rightarrow [(CP)^{-y}(Na^+)_y]_n + C_{10}H_8$

B. Electrochemical Doping

(a) p-type doping

$(CP)_n + [Li^+(BF_4^-)]_{soln} \rightarrow [(CP)^{+y}(BF_4^-)_y]_n + Li_{electrode}$

(b) n-type doping

$(CP)_n + Li_{electrode} \rightarrow [(CP)^{-y}(Li^+)_y]_n + [Li^+(BF_4^-)]_{soln}$

Figure 1.7 (A) Chemical doping and (B) Electrohemical doping in conjugated polymers.

The protonation of PANI is another example of chemical doping by acid-base chemistry. This process converts the semiconducting form of PANI to a metallic form of PANI (emeraldine base→emeraldine salt) [39]. The main disadvantage of chemical doping is the difficulty in controlling doping level. The electrochemical doping has the advantage of controlling the doping level by adjusting the working electrode (WE) potential with respect to the reference electrode (RE) (Figure 1.7 B) [40]. If the neutralization potential is not applied, the electrochemical doping produces stable charge carriers.

1.5 Measurement of Conductivity in Organic Materials

Increasing the conductivity of the same material to 8 or more orders is the unique property of CPs. Based on structures of polymers various conductivity mechanisms are available for CPs. Figure 1.8 represents the conductivity ranges for materials usually considered as metals, semiconductors and insulators. However, the factor that determines this classification is really the temperature dependence of conductivity rather than the conductivity itself. The conductivities of three conjugated polymers, polyacetylene, polypyrrole, and PTh shown in Figure 1.8, lie between the metallic conduction and insulator depending on the doping level. Since the band gap is generally greater than 3 eV, neutral polymers tend to be semiconductors or insulators. Doping by positive or negative charge carriers has a strong effect on conductivity.

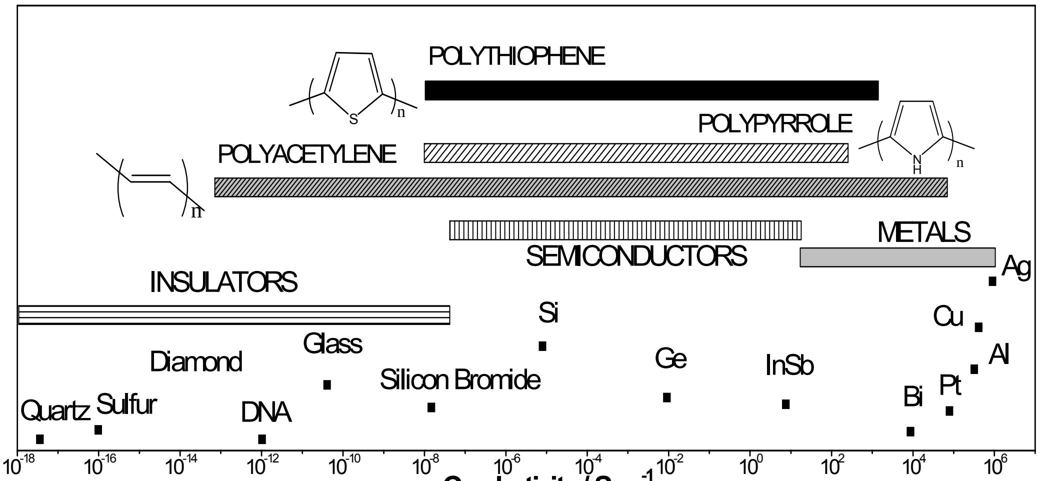

Figure 1.8 The conductivity range available to CPs [41].

1.5.1 Conductivity Measurements

Among the conductivity techniques used for measuring electrical conductivities of polymers, four probe methods have some advantages. In four probe methods the errors due to the contact resistance are eliminated since while the two contacts measure the potential difference, the others apply the current across the polymer sample. Also this method allows the application of conductivity measurements over a wide range of applied currents.

Free-standing polymer films are preferred for conductivity measurements because of their insolubilities. If a soluble polymer is used, the solution casting may be used for sample preparation. An alternative way of sample preparation for the insoluble and infusible polymers is the electrochemical polymerization to obtain thin films followed by polymer removal from the electrode by using a pressure sensitive adhesive tape.

There are three types of four probe methods that can be used for the measurement of conductivities of samples: (1) Van der Pauw [42], (2) four-wire [43], (3) four-point probe [44].

The Van der Pauw is a method used for irregularly shaped samples [42]. Cu or Ni wires are attached and contacts are achieved by silver paste in four points (*i, ii, iii,* and *iv*) located at the boundaries of the thin film (Figure 1.9 A).

Precise measurements can be achieved if the contacts are small enough and the thin film is homogeneous in thickness without any defects. If the contacts are positioned in a square form on the surface, the conductivity value is defined as:

$$\sigma = \ln 2\, (\pi R t)^{-1} \qquad (1.1)$$

where R is the sample resistance, and t is the thickness.

$$R = \Delta V / I \qquad (1.2)$$

Applied current and measured potential difference are defined as I and ΔV, respectively.

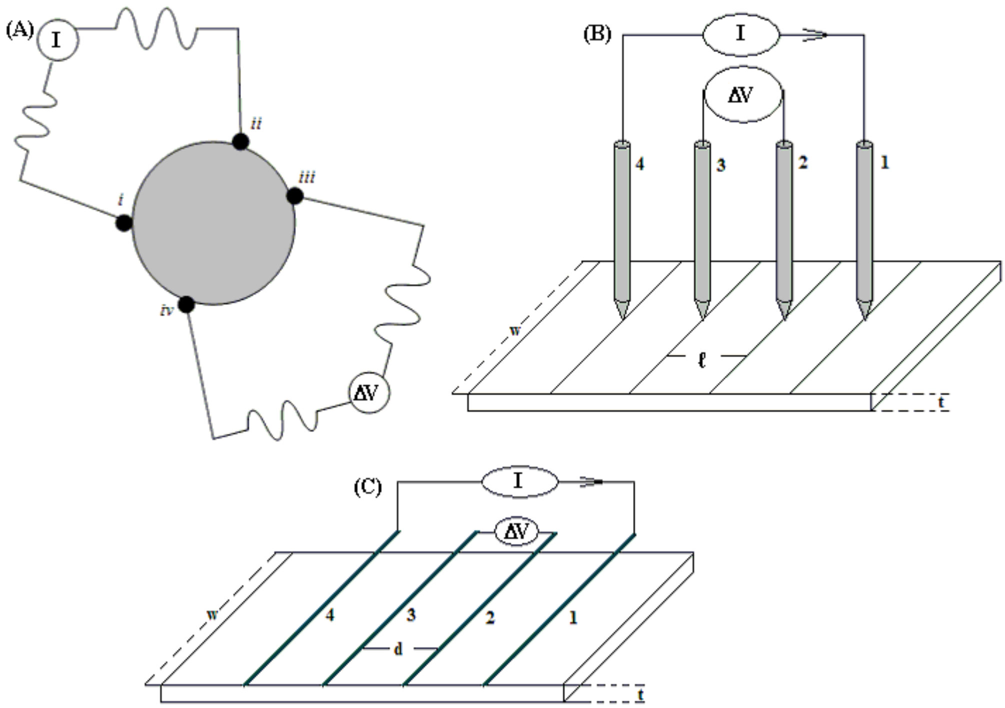

Figure 1.9 Four-probe conductivity methods: A) Van der Pauw, B) four-point probe, C) four-wire. (Adopted from [45])

Another method that employs devices with predefined electrodes is depicted in Figure 1.9 B showing the simplest form of a four-point probe measurement setup. A row of pointed electrodes touches the surface of a polymer film taped or spin cast on an insulating substrate. A known current, I, is applied between electrodes 1 and 4, while the potential difference, ΔV, is measured between electrodes 2 and 3. For this arrangement, the volume resistivity (ρ) of the sample is given by an equation derived by Valdes [46]:

$$\rho = 2\pi\ell \, \Delta V/I \qquad (1.3)$$

The result is independent of the electrode contact area as long as the distance between the points (ℓ) is much greater than the film thickness ($t \ll \ell$). Another equation for the resistivity of the film having a thickness t is:

$$\rho = (\Delta V/I)\,(t\,\pi/\ln 2)\,F \qquad (1.4)$$

where F (t/ℓ) is a correction factor.

In order to make low temperature conductivity measurements four-probe technique can be used instead of four probe device. The contacts are attached to the film, which is cut in a rectangular form, by using silver paste or vacuum evaporated metals. The width should be much smaller than its length. At low temperature measurements four thin Cu (or Au) wires are attached (Figure 1.9 C). Volume conductivity is calculated from the following equation:

$$\sigma = d/Rtw \qquad (1.5)$$

where d is the distance between contacts 3 and 2, t is the sample thickness and w is the width.

1.6 Nature of Conduction and Conduction Models

In CPs the conduction, unlike the inorganic semiconductors, is not an electronic conduction or ohmic conduction, because it is attributed mainly to charge carriers, such as bipolarons, not electrons. CPs are considered disordered semiconductors, and there are some theoretical conduction models for the explanation of conductivity in such amorphous structures. We are now in position to consider conduction models.

1.6.1 Mott’s Variable Range Hoping (VRH) Model

One of the first models to be considered for CPs, primarily because it appeared to apply to disordered conventional semiconductors and CPs were considered disordered, was that of Mott and coworkers [47]. This model correctly predicted the $T^{-1/4}$ dependence of conductivity observed in disordered semiconductors such as α-Ge. Lack of ordering in such materials was thought to produce localized electronic states similar to the localized states (structural distortions such as bipolarons) produced by short conjugation lengths in CPs. The model assumed that localization was not very strong and differed at different locations within a material, and thus postulated that conduction occurred through variable range hopping (VRH) of electrons between these localized sates. This electron hopping was assisted by phonons (lattice vibrations), and was somewhat dependent on the initial and final energies (overlap of wave functions) of the states between which hopping occurred, i.e. it was not isoenergetic. Another way to visualize phonon-assisted hopping is to picture charge hopping between two sites accompanied by a change of state of the lattice vibrations at both sites. This Mott VRH led to a general $T^{-1/4}$ dependence of the conductivity expressed by:

$$\sigma = \sigma_0 \exp\left(-\left(\frac{T_0}{T}\right)^{1/d+1}\right) \tag{1.6}$$

where:
d = dimensionality of material,

$$T_0 = \frac{\lambda \alpha^3}{k_B N(E_F)} \tag{1.7}$$

and

$$\sigma_0 = e^2 \upsilon R^2 N(E_F) \tag{1.8}$$

where σ_0, the localization length, is the length over which the wave function decays, k is the Boltzmann constant, $N(E_F)$ is the density of states at the Fermi level, and υ is the phonon frequency. A slight modification of this Mott VRH model, equating localization length with conjugation length in CPs and considering hopping between these rather than between point-like localizations, was proposed by Schäfer-Siebert and Roth [48] and yields;

$$\sigma = C(TT_0)^{-1/2} \exp\left(-\left(\frac{T_0}{T} \right)^{-1/2} \right) \tag{1.9}$$

with C being a constant.

The Mott's VRH model agrees well with experiment for moderate temperatures and doping levels for CPs, and is found to apply in many cases to materials such as amorphous carbon as well [49]. Indeed, many studies on a variety of CPs, such as those correlating ESR spins with dc conductivity [50], appear to confirm the Mott VRH model. Although there are two fitting parameters, σ_0 and T_0, the latter is found to be directly related to room temperature conductivity. In practice one usually tries to fit temperature vs. dc conductivity data to a $T^{-1/(d+1)}$ in order to get information about dimensionality of conduction.

1.6.2 Sheng Model

A model on a different basis for CPs was proposed by Sheng [51], which is applied to highly doped CPs. It assumes conduction between the metallic islands (highly conducting doped islands) within CPs discussed above, and yields the following temperature relation:

$$\sigma = \sigma_0 \exp(-T_1/(T + T_0)) \tag{1.10}$$

with T_1 being an additional fitting parameter, and this fitting parameter depends on the properties of the potential barriers (insulating islands) between the highly conducting islands. The potential barriers are also sometimes identified with interfibrillar spaces rather than insulating islands. The charge transport is said to result from tunnelling induced by thermal fluctuations. It is evident in this respect then that electronic overlap between different fibers, i.e. packing, would also affect conductivity. The above equation predicts a conductivity decreasing with temperature but still yielding a finite value at near absolute zero and a saturation value of conductivity at higher temperatures. The Sheng model applies well to highly doped or heterogeneous systems (such as PVC/CP composites), poorly at low temperatures, and poorly for low doping levels.

1.6.3 Kivelson Model

A model found to correctly predict the steep increase in conductivity of PA on doping and dependence of PA conductivity on temperature is proposed by Kivelson [52,53]. In its essence, this intersoliton hopping model applied primarily to polyacetylene proposes isoenergetic hopping of electrons from a neutral soliton of one chain to a charged soliton at a neighboring chain via tunnelling. It is able to account well for conductivity behavior of PA's at lower temperatures.

In practical applications the Mott VRH model is found to be widely applied to reasonable doping levels and also temperatures for all CPs, and for high doping levels, the Sheng model is found to fit well. The Kivelson model is applied within low limited doping and temperatures.

1.7 Applications of CPs

The novel properties of CPs are not typically available in other materials and these properties make many applications possible. These applications can be divided into three main classes. The first one uses conjugated polymers in their neutral form, and takes advantage of their semiconducting and luminescent properties. Examples of applications that use neutral polymers are conjugated polymers as semiconducting materials for field effect transistors [54] and as the active material in an electroluminescent device [55]. The second category of applications involves using the polymer in its doped or conducting form, and some representative applications in this category are electrostatic charge dissipation and EMI shielding [7,56], selective anionic membranes and capacitors [9]. The third category uses the ability of the polymer to reversibly switch between its conducting and reduced forms. Upon switching between these two states, the polymer undergoes color, conductivity, and volume changes. Applications that use these properties include battery electrodes [57], mechanical actuators [58], sensors [59], drug delivery [60], and electrochromics [55].

1.8 Crown Ether or Polyether Substituted CPs

The crown ethers (CE) defined as uncharged macroheterocycles containing the repeat unit (–O–CH_2–CH_2–)$_n$ (Figure 1.10) were discovered in 1967 by Pedersen [61,62]. Their structures are suitable to make complex with cations of alkali and alkaline earth elements, transition metals, and also ammonium ion.

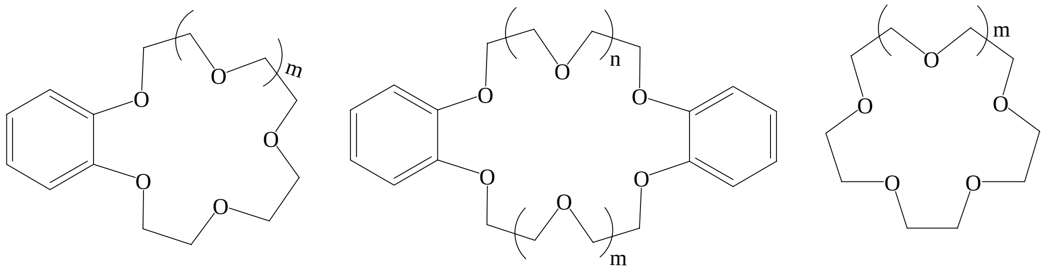

m=1 benzo-15-crown-5
m=2 benzo-18-crown-6

n=0, m=0 dibenzo-12-crown-4
n=1, m=0 dibenzo-15-crown-5
n=1, m=1 dibenzo-18-crown-6
n=2, m=2 dibenzo-24-crown-8

m=0:12-crown-4
m=1:15-crown-5
m=2:18-crown-6

Figure 1.10 Some examples of CES and related compounds.

In addition to the chemistry of the crown ethers [63,64,65], their analytical, chemical, and biological applications have been reported [66] in several review papers. Furthermore, the benefits of functionalized crown ethers in the applications of analytical chemistry and related fields were also summarized by M. Takagi and H. Nakamura [67].

The complexing properties of crown ethers depend on the physical properties of both the crown ethers and the ion being complexed. Some factors affecting the complexing properties of crown ether can be explained by the electrical charge of the ions, the number and type of heteroatoms in the ring, the relative sizes of the ions and the hole in crown cavity, etc. [61].

When the ionic diameter is closely equal to the crown diameter, the most stable complexes are usually formed [68,69]. In this situation, the stoichiometry of the complex is 1:1 with the cation assumed to be surrounded by the cavity of the polyether ring. When the diameter of cation is larger than that of cavity, 1:2 and 2:3 complexes are formed.

Although crown ether containing molecules are well documented due to above mentioned properties, their polymers are also of great interest since such polymers are good candidates for the extraction of metal ions. For example, dibenzo-18-crown-6 is a macrocyclic monomer and its conductive polymer films have complexing properties towards cations especially in their reduced form. Its electrochemical polymerization was reported by V. Le Berre for the first time [70]. Later on, the same group reported that the best condition for the formation of conducting polymer films from dibenzo-18-crown-6 is using a mixture of dichloromethane/acetonitrile (1/1, v/v) as solvent [71]. Cihaner et al. investigated anodic polymerization of dibenzo-18-crown-6 in the same solvent mixture using in-situ ESR and in-situ UV-VIS spectroscopic techniques [72].

1.8.1 Polyether Substituted PTh

The oxidation of starting monomer substituted by a group containing polyether produces functionalized CPs. These conjugated polymers can be used for constructing cation-responsive electrodes. Therefore, interaction between the cation and the polyether bridge is possible. Consequently, recognition of a different class of cations including alkali, heavy and precious metal cations are achieved by some of these polymers.

The PTh films containing oligo(oxyethylene) (polyether) chains have significance not only due to their tendency to form complex with cations, but also due to their better solubility and high hydrophilicity [73]. Two principal conditions must be achieved for the electrochemical synthesis of such functionalized polymers. Firstly, two or more -CH_2 groups must exist as a spacer between the Th rings and the first oxygen atom in order to neutralize the electron-withdrawing effect of ether groups on the conjugated system [74]. The presence of one methylene group separating the first oxygen atom from the heterocycle causes a decrease in conjugation and the conductivity of the corresponding polymer due to an increase of the oxidation potential of the monomer. Secondly, the difficulty in the electrochemical polymerization of the monomer caused by the steric bulkiness of the functional group can be eliminated if the polyether chain is not too long. As reported by Lemaire et al. [74] polymerization of the Th, which is substituted by more than seven ether groups, was not successful.

By achieving these two conditions, the electropolymerization of polyether-substituted thiophenes (Ths) could be potentiostatically or galvanostatically realized to obtain electroactive polymers. The electrosynthesis medium was generally nitrobenzene or acetonitrile containing perchlorate, tetrafluoroborate, or hexafluorophosphate salts as the supporting electrolytes and also the most homogeneous and conducting PTh films were synthesized by galvanostatic conditions [73].

A considerable increase in hydrophilicity has been observed in polymer **1** (Figure 1.11) and the polymer remains electroactive in aqueous media, in contrast to poly(alkylthiopehene)s [74,75]. This was the first conjugated polymer system with a covalently attached polyether group for ion complexation. Also, this polymer shows a specific electrochemical response to Li^+.

On the other hand, the symmetrical monomers having two Th rings linked by a polyether unit have been synthesized and their electrochemical behaviors have been investigated [76,77,78]. Electrochemical polymerization of 2**b** (Figure 1.11) is performed in the presence of lithium ion in an effort to template intramolecular coupling and macrocycle closure. The electrical conductivities of these polymer films were reported in the range of 10^{-2} S/cm. However, its structure and its sensing properties were not determined [76]. The complexation properties of various neutral poly(**2**) toward inorganic cations (Ag^+, Mn^{2+}, Co^{2+} and Sb^{3+}) have been studied and the results revealed that the binding power of these polymers towards Mn^{2+} and Co^{2+} is much stronger than their binding power towards Sb^{3+} [79].

Another study about α-and β- substituted polyether bridged Th rings was reported by our group [80]. The cleavage of the polyether bridge during polymerization was observed at α - substituted monomer.

The synthesis of acyclic polyether chain substituted at -α position of Th derivatives **3** (Figure 1.11) were reported by Simonet and co-workers. Unlike the Ths functionalized in the -β position, the oxidation of such compounds produced unconjugated redox-type polymer films, except for 3**e** and 3**f** of which polymers were not synthesized. The oxidation potential of the monomers bearing the R group was found to be dependent on the electronic character of the R. Therefore, while the **3e** and **3f** were oxidized at a lower potential than **3a,** due to the presence of the electron-withdrawing nitro group, **3d** was oxidized at a higher potential than **3a**.

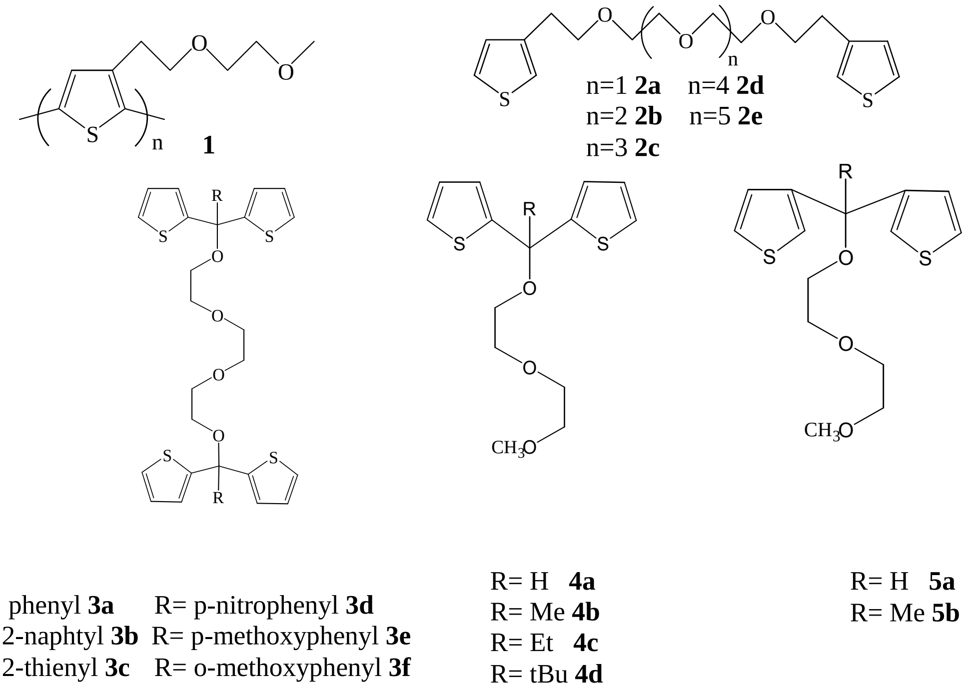

Figure 1.11 Some examples of oligo(oxyethylene)-substituted Ths.

The chemical and the electrochemical properties of the compound **4** and **5** (Figure 1.11) were studied by Marrec et al. [81] and they reported that the resulting polymer obtained from **4,** after the electrolysis, contains high sulphur ratio found by elemental analysis. The possible cleavage of the ether chain, followed a β-elimination reaction, by might be the reason, due to the decrease in bond strength between the benzylic carbon and oxygen at the stage of the radical cation [81]. On the other hand, oxidation of monomers of **5a** and **5b** were achieved at 1.7 vs. 0.1 M Ag^+/Ag and electroactive polymer films were synthesized on the electrode surface without any cleavage.

All these polymers showed two reversible redox systems corresponding to the n-doping and p-doping. They exhibited stable electroactivity during transition between both states. Even though the possible tendency to form complex with some cations have not yet been studied, the ability of this type of polymers being negatively and positively charged should be of great interest for the development of chemically reversible ionic sensors.

1.8.2 Polyether Substituted PANIs

Although there are a large number of studies about polyether substituted PThs, there are very few studies on PANI functionalized by polyethers. Kitani and co workers have reported the synthesis and properties of PANI containing two (**6a**) or three (**6b**) oxyethylene units in the polymer side chain (Figure 1.12) [82,83]. In addition to this we have described [84] the electrochemical polymerization of *ortho* substituted polyether bridged aniline derivatives. However, it was found that the polymers have poor conductivities.

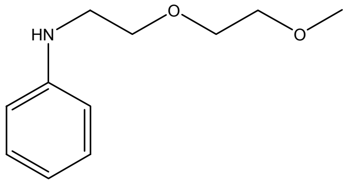

n=1:**6a**

n=2:**6b**

Figure 1.12 Polyether substituted aniline derivatives.

The synthesis of N-substituted PANI derivatives were achieved in acetonitrile solution including sulphuric acid as a supporting electrolyte. The electrochemical properties such as redox behavior during n- and p-type doping processes were investigated. The conductivities of these polymers were also found in the range of 10^{-3} S/cm.

1.9 Stripping Analysis

Stripping analysis is a very sensitive electrochemical method for measuring the trace metals [85,86,87]. Its sensitivity is attributed to the combination of more complicated measurement procedures that produces a very high signal/background ratio and the preconcentration (or deposition) step. Due to the preconcentration of the metals on the electrode by factors of 10^2–10^3, detection limits are lowered by the same factor compared to solution-phase voltammetric techniques and various metals can be analyzed simultaneously at concentrations about 10^{-11} M. Different stripping techniques are available and can be utilized in detecting metal ions. The most important thing is to achieve sufficiently high currents and reproducible results. Therefore, any of the following methods can be used for detection such as, normal pulse stripping voltammetry, square wave pulse stripping voltammetry, differential pulse stripping voltammetry, linear sweep stripping voltammetry etc.

1.9.1 Anodic Stripping Voltammetry (ASV)

Anodic stripping voltammetry is a well-known electrochemical method which is very appropriate for quantitative detection of trace metals due to its sensitivity, relatively simple instrumentation, low maintenance costs, and minimum sample pretreatment prior to analysis.

The enhanced sensitivity and lower detection limits can be achieved in this technique by enrichment of the analyte prior to voltammetric determination. The common enrichment processes include reduction of metal ions through formation of metal films or amalgams, reductive or oxidative formation of sparingly soluble salts with or without reagent addition, and adsorptive accumulation of chelates or complexes onto the electrode surface.

In anodic stripping voltammetry the current flow between working electrode (WE) and counter electrode (CE) is measured as a function of the potential applied to WE. In enrichment process during ASV, a cathodic potential is applied to the WE to reduce the desired metal ions. During this deposition step the potential is kept constant. Deposition process also requires stirring to achieve transport of the metal ions from bulk solution to the diffusion layer (Figure 1.13).

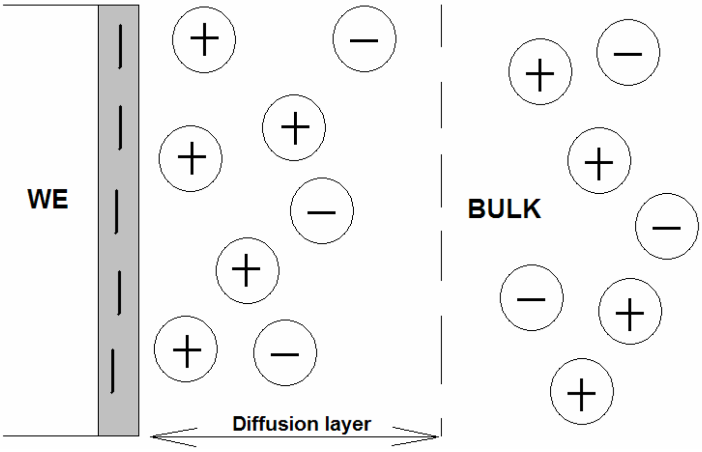

Figure 1.13 Structure of the electrode-solution interface and double layer.

The second step is the stripping step where the metal ion detection is achieved after accumulation is completed. In this process the WE is scanned in positive direction from deposition potential. As the potential increases, the accumulated metal will be oxidized at its oxidation potential. Oxidation is followed by stripping of the metal ion from the electrode surface. The current vs. potential voltammogram is generated through the stripping step. The current measured during stripping is proportional to the metal ion concentration in medium. The potential-time sequence for an anodic stripping voltammetry can be seen in Figure 1.14.

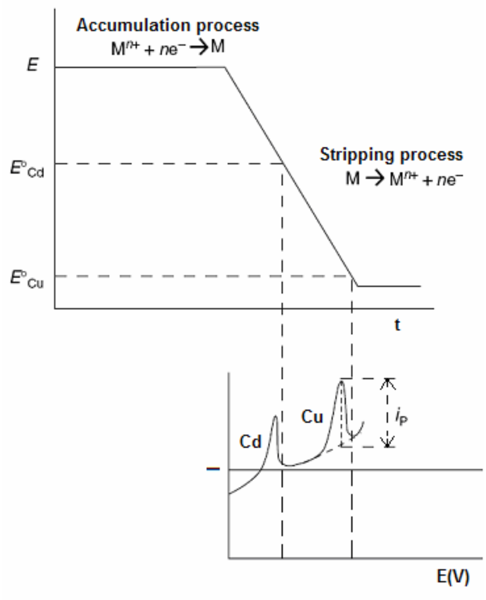

Figure 1.14 Potential-time waveform of ASV and resulting voltammogram.

The low detection limits in ASV are possible because of the deposition step; however, the mechanism by which metal deposition occurs can also affect the detection limit. Many metals, such as lead [88,89,90], copper [90], mercury [91, 92], and silver [91] deposit onto WEs according to a nucleation and growth mechanism. This mechanism states that certain sites on the electrode are more active toward metal deposition than others. The metal ion deposits onto these more active sites. The nuclei growth follows this process on the electrode.

The detection limit in ASV is also affected by the stripping step. Although the potential of the WE electrode can be scanned linearly during the stripping step, pulsed waveforms are often used to reduce the background current.
To conduct an experiment in ASV, a three electrode cell is needed, as shown in Figure 1.15. The reaction of interest occurs at the working electrode to which the deposition potential and stripping waveform are applied.

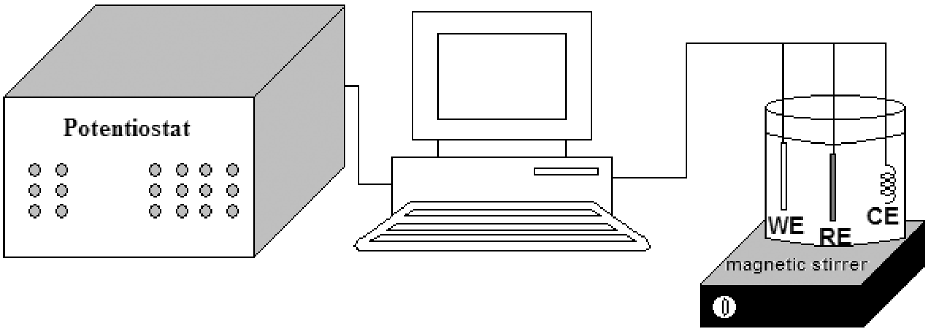

Figure 1.15 The three-electrode cell and software assisted power source used in DPASV.

Briefly, ASV has excellent detection limits for trace metal analysis, because preconcentration (or deposition) can occur for as long as desired. ASV experiments are performed in a three-electrode cell, and the important variables that can be controlled are the deposition time and potential, and the stripping parameters.

1.9.2 Electrodes for Stripping Analysis

A proper choice of the WE is important for the success of the stripping operation. In particular conventional mercury electrodes (the mercury film electrode and hanging mercury electrode) have been very popular for stripping voltammetry. However, due to its toxicity, the use of mercury is now highly avoided. Therefore, various mercury-free electrodes including gold coated electrodes [93,94], silver electrodes [95,96], glassy carbon electrodes [97,98], carbon paste electrodes [99,100,101], carbon nanotube electrodes [102] or screen-printed carbon electrodes [103,104] have been considered for sensitive metal determinations.

1.10 Aim of This Study

Polyether substituted PThs and PANIs are interesting polymers because of their complexing properties towards cations of different sizes. However, polyether bridged PThs and PANIs would be more interesting since polymer chains would probably contain cavities of various sizes, depending on the polyether bridge length. One can find some examples of such polymers having polyether bridges between Th or Py rings. However, there are no examples of polyether bridged PANIs in the literature. In this study one of our aim was to synthesize new monomers containing polyether bridges between two heterocyclic monomers (i.e Th and ANI). Since their polymers possibly would contain cavities into which various cations can be localized. We have also studied their electrochemical polymerization including detailed investigation of the electrochemical behavior of the synthesized monomers and polymers. The possible application of the polymers in detecting some metal ions was also studied. In addition, electrochemical and spectroelectrochemical behaviors of the conducting copolymers of the polyether bridged aniline monomers with aniline were studied and electrical conduction mechanism was investigated in detail.

CHAPTER 2

EXPERIMENTAL

2.1 Materials

The supporting electrolyte, tetrabutylammonium hexafluorophosphate (TBAPF6) (Aldrich) was used without further purification. Acetonitrile was firstly dried over CaH_2 and distilled once from P_2O_5 under Ar(g) and stored over molecular sieves. Dichloromethane was also dried over CaH_2 and distilled over CaH_2 under nitrogen. Two solvents were treated with freshly activated alumina prior to use. Tetrahydrofuran (THF) was refluxed with sodium/benzophenone and distilled under Ar(g) atmosphere. NaH (Riedel-de Haen, 60% suspension in oil), 3-carboxyaldehyde Th (Aldrich) was used as received. Aniline was freshly distilled before use. Polished platinum electrodes and glassy carbon electrode were used as WE and counter electrodes. For SPEL studies indium tin oxide coated quartz glass (ITO) (Delta Tech. 8-12 Ω) , was used as WE. Solvent mixture was purged with Ar(g) for 30 min prior to SPEL studies and the measurements were done under Ar(g) atmosphere. In order to avoid the diffusion of water, Ag-wire was preferred as RE for electrochemical polymerization and for CV, respectively.

2.2 Cyclic Voltammetry (CV) and Constant Potential Electrolysis (CPE)

A large variety of electroanalytical methods can be applied to the study of conducting polymers. Among them CV is the most popular due to its simplicity and versatility in studying the redox behavior of the monomer and polymer. Furthermore, CV reveals information regarding the stability of the product during multiple redox cycles.

This method sweeps the potential of an electrode, immersed in an unstirred solution, and measuring the resulting current flow between WE and CE. Therefore, the obtained voltammogram is a display of current (vertical axis) vs. potential (horizontal axis).

The reducing or oxidizing strength of the WE is precisely controlled by the applied potential. Continuous deposition of CP onto the WE can be monitored by the increase in the polymer's anodic and cathodic peak currents, while the polymer redox properties are characterized by the magnitudes of its peak potentials.

CV and electrolysis experiments were carried out by a Gamry potentiostat (equipped with PHE 200 Physical Electrochemistry software), utilizing a three-electrode configuration. Prior to electrochemical polymerization, electrolytic solution was purged with Ar(g) for oxygen removal. The solution was kept oxygen-free during electrochemical measurements by passing Ar(g) over the solution. Following electropolymerization, redox behaviors of the polymer films were investigated in monomer free electrolytic solutions.

2.3 Spectroelectrochemistry

SPEL measurements provide information about the material's band gap and intraband states created upon doping as well as the electrochromic properties of CPs at various applied potentials.

SPEL measurements were carried out with a HP 8453A diode array UV-VIS spectrometer using a specially designed three-electrode cell to allow potential application while monitoring the absorption spectra. The WE is an ITO fitting a SPEL cuvette (0.7 cm wide). Ag-wire pseudo reference is used as a RE and a Pt wire is used as a counter electrode. For potential control, all three electrodes were connected to a Gamry potentiostat (equipped with PHE 200 Physical Electrochemistry software).

2.4 Spectroscopic Measurements

FTIR spectra and ^{13}C-, ^{1}H-NMR spectra of the polymers were recorded on a Bruker Vertex-70 FTIR spectrophotometer and a Bruker Instrument-NMR Spectrometer (DPX-400), respectively. Varian E12 ESR spectrometer was used for investigating paramagnetic behavior of the polymers and also for in-situ studies. Thermal characterization of polymers was carried out using a Perkin Elmer TGA system under air.

2.5 Electrical Measurements

Among available conductivity techniques, four-probe method has several advantages for measuring electrical properties of conducting polymers. First, four-probe technique eliminate errors caused by contact resistance, since the two contacts measuring the voltage drop are different from the contacts applying the current across the sample. Second, this technique allows for conductivity measurements over a broad range of applied currents, usually varying between 1 μA and 1 mA for conducting polymers studied in this work. These current values produce potential differences ranging from 10 μV to 10 V, depending on the resistance and thickness of the sample. For the electrical characterization of polymer films, dc resistivity measurements were performed at room temperature and also in the temperature range of 100-300 K were measured. The details of the measurement techniques are described in the following section.

2.5.1 Conductivity Measurement

The resistivity of the samples was measured by applying the standard dc-technique and four-probe method. The temperature variation of resistivity in between 100-300 K range was studied by placing the samples in a closed cycle nitrogen cryostat. For the electrical measurements the constant current was applied to the samples by using a Keithley 6220 programmable current source and the voltage drops were measured by a Keithley 6514 electrometer.

The variation of the current range depends on the total resistivity of the sample studied, the electrical resistivity was obtained by using the following expression,

$$\rho = \frac{wtV}{LI} \qquad (2.1)$$

where w is the width of the thin film, t is the thickness, L is the spacing of the contacts across which the voltage is measured and V/I is the inverse slope of I-V characteristics. Note that the current $I_{1,4}$ versus the voltage $V_{2,3}$ slope is taken as the slope of I-V characteristics. The equation is not valid unless the contacts are ohmic, therefore the ohmicity of contacts must be checked by plotting the logarithmic I-V characteristics where the slope has to be around unity for both polarities, which means that the voltage current relationship is linear satisfying the Ohm′s law.

The temperature dependence of resistivity has been studied by the measurements performed on the samples placed in Janis cryostat and Lake Shore 331 temperature controller in the temperature range of 100-300K, within 5 or 10 K (±0.1K) intervals.

2.6 Synthesis of Monomers

2.6.1 Synthesis of 1,12-di-3-thienyl-2,5,8,11-tetraoxadodecane (MI) and 1,15-di-3-thienyl-2,5,8,11,14-pentaoxapentadecane (MII)

The 3-carboxyaldehyde Th (25 mmol) was dissolved in methanol (50mL) and cooled to 0 °C. Then, 25 mmol of $NaBH_4$ was gradually added and the resulting solution was stirred for 30 min. After this period the solution was diluted with water and extraction was done by diethyl ether and the trace amount of water was dried with $MgSO_4$. Evaporation of diethyl ether yielded 3-thienyl methanol (90%).

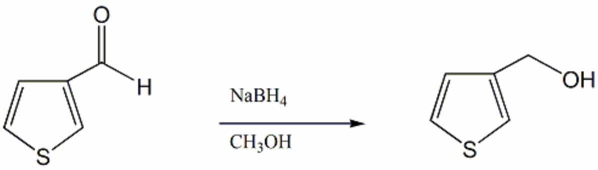

Figure 2.1 Reduction of 3-carboxyaldehyde Th.

The monomers in Scheme 2 were synthesized according to a general procedure described in the literature [105]. 20 mmol 3-thienyl methanol and excess NaH were mixed in 200 mL of dry THF under Ar(g) atmosphere for 30 min at room temperature. 19.5 mmol of ditosylate (with the appropriate chain length) were added drop wise over an hour and the solution was refluxed for 24 hours. Then, the hot solution was cooled to room temperature and neutralized by 0.1 M HCl until a clear yellow solution was obtained. The solution was extracted by diethyl ether or CH_2Cl_2 and washed with water. The organic phase was dried over $MgSO_4$ and evaporated under reduced pressure to yield an oily residue. Its chromatographic purification on a packed silica gel using hexane/ethyl acetate as an eluent afforded monomers as clear yellowish oils. ^1H and ^{13}C-NMR spectra were recorded in $CDCl_3$ and are given in ppm with respect to TMS (Figure 2.2.).

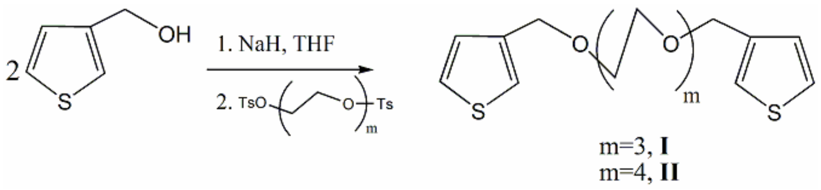

Figure 2.2 Synthesis of **MI** and **MII**.

2.6.2 2,2'-[ethane-1,2-diylbis(oxyethane-2,1-diyloxy)]dianiline (MIII) and 2,2'-[oxybis(ethane-2,1-diyloxyethane-2,1-diyloxy)]dianiline (MIV)

The syntheses of 2,2'-[ethane-1,2-diylbis(oxyethane-2,1-diyloxy)]dianiline (**MIII**) and 2,2'-[oxybis(ethane-2,1-diyloxyethane-2,1-diyloxy)]dianiline (**MIV**) were achieved according to the procedure described in the literature [106].

Ditosylate with the appropriate chain length (86 mmol) was added to a mixture of 2-nitrophenol (172 mmol) in DMF (200 mL). After being stirred and heated to reflux for 16 hours, the resulting solution was partially concentrated under reduced pressure and then poured into 750 mL of water. The precipitate was collected, washed with water, and recrystallized from methanol to give 60%, 51.6 mmol of tri- or tetraethylene glycol bis(2-nitrophenyl ether).

A solution of 25.5 mmol of tri- or tetraethylene glycol bis(2-nitrophenyl ether) in ethanol (180 mL) was warmed until complete dissolution. Catalyst (1 g of 5% Pd-C) was then added, and hydrazine monohydrate (153 mmol) was slowly added from an additional funnel. The mixture was refluxed for 1 hour and then filtered through a pad of celite. The solvent was removed under reduced pressure, and the residue recrystallized from methanol–diethyl ether at -20 ^{o}C to give 80% 20.4 mmol of product.

2.7 Polymerization Methods

2.7.1 Electrochemical Polymerization

Electrochemical polymerizations were performed in a classical three-electrode cell. The platinum sheets, glassy carbon electrode, and ITO coated quartz electrodes were used as WE. Counter electrode was a rectangular platinum sheet. Ag-wire, SCE, and Ag/AgCl were used as reference electrodes.

Polymers of Th derivatives were grown using constant potential electrolysis (oxidation potential of related monomer) in 0.1 M TBAPF6 solution containing 0.05 M of monomer. Samples were peeled off from the WE, washed with CH_3CN and then dried under vacuum at 50 ^oC for 12 h.

Polymerizations of aniline derivatives were achieved in 3.0 M H_2SO_4 in water by cyclic voltammetry technique. Polymer films were peeled off from the ITO coated quartz electrode, washed with water and then dried under vacuum at 60 ^oC for 12 h.

2.7.2 Chemical Polymerization

The related monomer (125 mmol) was dissolved in 200 mL of 1.0 $molL^{-1}$ HCl(aq) solution. The solution was kept at 0–5 ^oC in an ice bath. A pre-chilled solution of 125mmol of $(NH_4)_2S_2O_8$ in 50 mL of 1.0 $molL^{-1}$ HCl(aq) solution was added slowly with vigorous stirring. The reaction mixture was agitated continuously for another 5 h at 0–5 ^oC. The precipitate was filtered and washed with 1.0 $molL^{-1}$ HCl(aq) until the filtrate become colorless. Upon rigorously drying under vacuum for 48 h at 60 ^oC, a black powder was obtained with a yield of 70%.

2.8 Cation Analysis by Differential Pulse Anodic Stripping Voltammetry

2.8.1 Preparation of Modified Glassy Carbon Electrode

Prior to polymer film deposition, the GCE was polished with 1 μm, 0.25 μm, and 0.1 μm diamond slurry, respectively. After each polishing step the electrode was rinsed with deionized water and sonicated in methanol and deionized water for 3 min. The electrode was pretreated by cycling in 3.0 M H_2SO_4. This procedure was repeated before each new set of cation analysis experiments.

Monomer **MIII** (0.05 M) was polymerized on GCE, in 3.0 M H_2SO_4 solution. Polymer film coated GCE was rinsed with acid solution and deionized water.

In order to obtain differential pulse stripping voltammograms the following procedure was applied. Lead, cadmium, and copper stock solutions were prepared in 10^{-2} M HNO_3. For each experiment 20 μL of desired cation solution was added to the voltammetric cell containing 0.2 M acetate buffer. Prior to analysis the stirrer was switched on and the solution was purged with nitrogen for 10 min to get deoxygenated solution. After purging, accumulation potential of -1.2 V was applied to modified GCE for 120 s and at the end of this period the stirrer was stopped and before voltammetric analysis 30 s break was given to get quiescent solution. The differential pulse anodic stripping voltammetry detections were done by sweeping potential from -1.2 to -0.2 V with a pulse height of 25 mV, a pulse time of 20 ms, a step size of 5 mV, and the sample period of 0.2 s. Before new analysis purging with nitrogen was repeated for 30 s with stirring after each new addition. Before the repeated measurements at the same modified GCE, the stirrer was switched on and the potential of +0.2 V was applied to the working electrode for 60 s while purging with nitrogen to get rid of all deposited metals.

CHAPTER 3

RESULTS AND DISCUSSION

3.1 Polymers of 3-Substituted Thiophene Derivatives Linked by Polyether Bridges

3.1.1 Synthesis and Characterization of 1,12-di-3-thienyl-2,5,8,11-tetraoxadodecane (MI) and 1,15-di-3-thienyl-2,5,8,11,14-pentaoxapentadecane (MII)

1,12-di-3-thienyl-2,5,8,11-tetraoxadodecane (**MI**) and 1,15-di-3-thienyl-2,5,8,11,14-pentaoxapentadecane (**MII**) were synthesized according to literature [105]. ^{1}H and ^{13}C-NMR spectra were recorded in $CDCl_3$ and are given in ppm referred to TMS and the chemical shifts were as follows.

3.1.1.1 Characterization of MI by NMR Spectroscopy

Clear yellowish oil. Yield: ~70%. ^{1}H NMR (400 MHz in $CDCl_3$) d/ppm: (m, J (Hz)): 3.52–3.63 (m, 12H), 4.48 (s, 4H), 6.97 (dd, J = 4.28 Hz, 2H), 7.11 (d, J = 2.22 Hz, 2H), 7.19 (m, 2H).

^{13}C NMR 100 MHz ($CDCl_3$) d/ppm: 139.92, 127.65, 126.13, 122.95, 71.03, 69.74, 68.77.

3.1.1.2 Characterization of MII by NMR Spectroscopy

Clear yellowish oil. Yield: ~70%. ^{1}H NMR (400 MHz in $CDCl_3$) d/ppm: (m, J (Hz)): 3.51–3.58 (m, 16H), 4.48 (s, 4H), 6.97 (dd, J = 4.87 Hz, 2H), 7.11 (d, J = 1.84 Hz, 2H), 7.19 (m, 2H).

^{13}C NMR 100 MHz ($CDCl_3$) d/ppm: 139.43, 127.25, 125.74, 122.61, 70.61, 70.52, 69.29, 68.38.

3.1.2 Electrochemical Behavior of MI and MII

Electrochemical behavior of monomers, **MI** and **MII,** were investigated in 0.1 M TBAPF6/CH_3CN solution utilizing cyclic voltammetry. The electrochemical data obtained for both monomers are tabulated in Table 3.1 and CVs are depicted in Figure 3.1. Both **MI** and **MII** exhibit one irreversible oxidation peak during the first anodic scan at 2.10 and 2.05 V vs. SCE, respectively. However, a new reduction peak was also observed at about 1.00 V vs. SCE, during the reverse scan. This reduction peak is accompanied with an oxidation peak, forming a reversible couple, which intensifies during repetitive cycling. This observation is characteristic for the formation of conducting polymer deposits on the working electrode surface (see Figures 3.1 (b) and (d)).

Since the polyether unit is known to be electrochemically inert up to 2.0 V [16], the anodic peak observed in the CV of monomers is most probably due to electron loss from the Th ring. This results in the formation of a radical cation localized in the Th ring which undergoes further reaction yielding the polymers poly(**I**) and poly(**II**) from **MI** and **MII**, respectively. It is also important to mention that the length of polyether spacer has little effect on the anodic peak potential values of the monomers. This is not surprising since the oxygen atom of the polyether spacer is not directly attached to the five-membered aromatic ring.

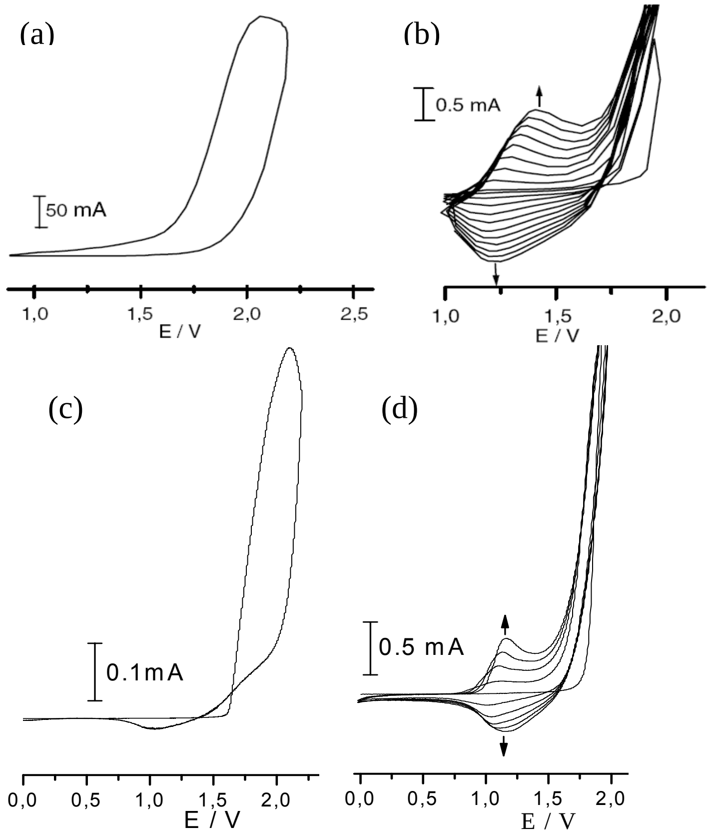

Figure 3.1 CVs of: (a) 10^{-3} M **MI**, and (b) repetitive cycling of 10^{-2} M **MI** (c) 10^{-3} M **MII**, and (d) repetitive cycling of 10^{-2} M **MII** in an electrolytic solution containing 0.1 M TBAPF6 dissolved in CH_3CN vs. SCE (scan rate = 100 mVs^{-1}).

Table 3.1 CV data for **I**, **II**, poly(**I**), and poly(**II**) vs. SCE.

Monomers	Monomer		Polymer	
	E_{pa}(V)		E_{pa}(V)	E_{pc}(V)
MI	2.1	Poly(**I**)	1.14	1.01
MII	2.05	Poly(**II**)	1.12	0.95

3.1.3 Polymer Synthesis and Characterization

Although repetitive cycling of both monomers resulted in the formation of polymer film on the working electrode surface, the preparative formation of polymers, poly(**I**) and poly(**II**), were achieved in the same solvent/electrolyte using 1.0 cm^2 Pt-plates as the working and counter electrodes. Constant potential electrolysis, at 1.90 V vs. SCE, was used for this purpose. The bright black film formed at the end of CPE was peeled off from the WE surface and dried under vacuum after washing with ACN.

3.1.3.1 Electrochemical Behavior of Poly(I) and Poly(II)

The electrochemical behaviors of polymer films were investigated in monomer-free electrolyte solution. Both polymer films were found to exhibit one reversible redox couple representing the doping and de-doping of the polymer films at about 1.00 V vs. SCE. It is well-known that both the anodic (i_{pa}) and cathodic (i_{pc}) current responses must change linearly with voltage scan rate when the electroactive species are electrode-confined. Therefore, the electrochemical behavior of poly(**I**) coated on WE (100 mC) was investigated at different voltage scan rates and the results are depicted in Figure 3.2. It is found that both anodic and cathodic peak currents increase linearly with increasing scan rate, indicating that the redox process is non-diffusional and the electroactive centers of the polymer are well adhered to the working electrode.

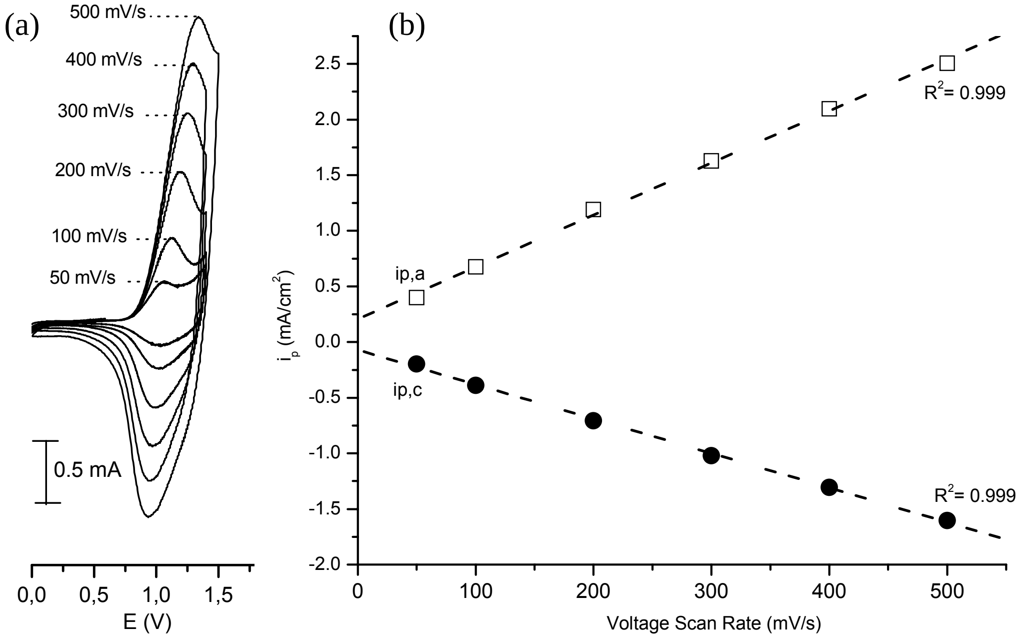

Figure 3.2 (a)Cyclic voltammograms of poly(**I**) with different scan rates, (b) Anodic (i_{pa}) and cathodic (i_{pc}) peak heights versus voltage scan rate (v) in monomer-free electrolytic solution containing 0.1 M TBAPF6 dissolved in CH_3CN.

3.1.3.2 FT-IR Analysis

Characterization of the resulting polymer was carried out using FT-IR spectroscopy (Figure 3.3). A close inspection of Figure 3.3 indicates that FT-IR spectrum of the poly(**I**) exhibits all characteristic peaks of the corresponding monomer together with an intense peak at about 840 cm^{-1} attributed to PF_6^- dopant anion. The peaks at 2865 and 1098 cm^{-1} are attributed to the polyether groups and their presence, contrary to what was found for monomers **MI** and **MII**, indicates that polyether bridges are not broken during the electrochemical polymerization of **MI** and **MII**. Also, the 800 cm^{-1} peak corresponds to α–ά coupling between Th rings. The proposed structure of poly(**I**) can be seen in Figure 3.4.

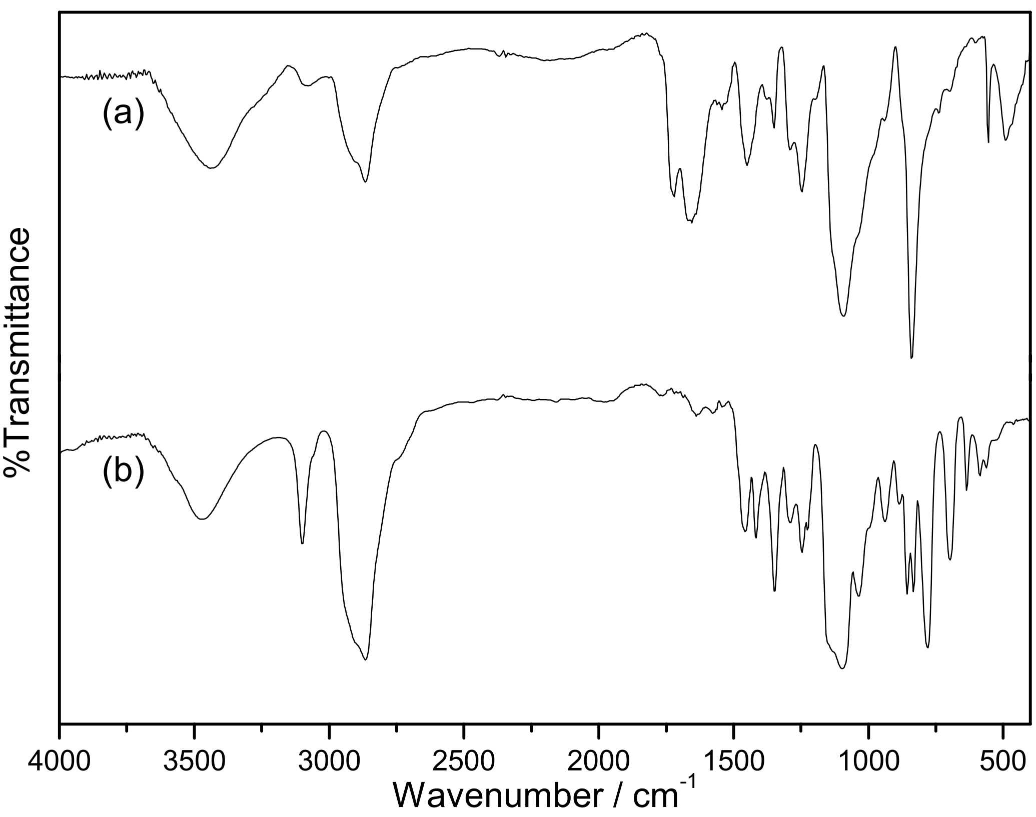

Figure 3.3 FT-IR spectra of: (a) Poly(**I**) and (b) **MI**.

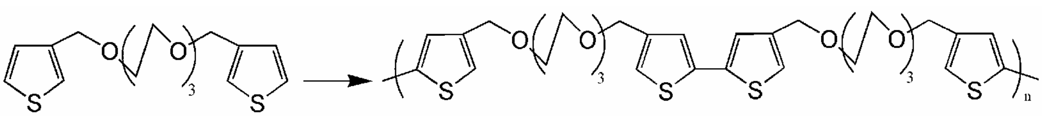

Figure 3.4 Proposed structure of electrochemically synthesized Poly(**I**).

3.1.3.3 ESR Study

Although the CVs of monomers, **MI** and **MII,** exhibit an increasingly intense new peak, characteristic of a conducting polymer film, after the first positive scan the fresh polymer film obtained via CPE at 1.9 V was found to lose its conductivity after a short period of time. However, its conductivity can be increased by I_2 doping. Therefore, we have also monitored the doping process by recording the ESR spectrum of the polymer film in situ during I_2 doping. As seen from Figure 3.5, the intensity of the ESR signal (ΔH = 0.83 mT) is increased during the doping process, indicating an increase in the number of polarons formed. However, the intensity of signal starts to decrease gradually after ceasing the I_2 vapor. The loss of conductivity in the freshly prepared film and the decrease in the ESR signal intensity after stopping the doping process indicated that polymer film is more stable in the neutral state than in the oxidized state. This might be due to the higher sensitivity of the polymer film to moisture because of the presence of the polyether spacer in the polymer backbone.

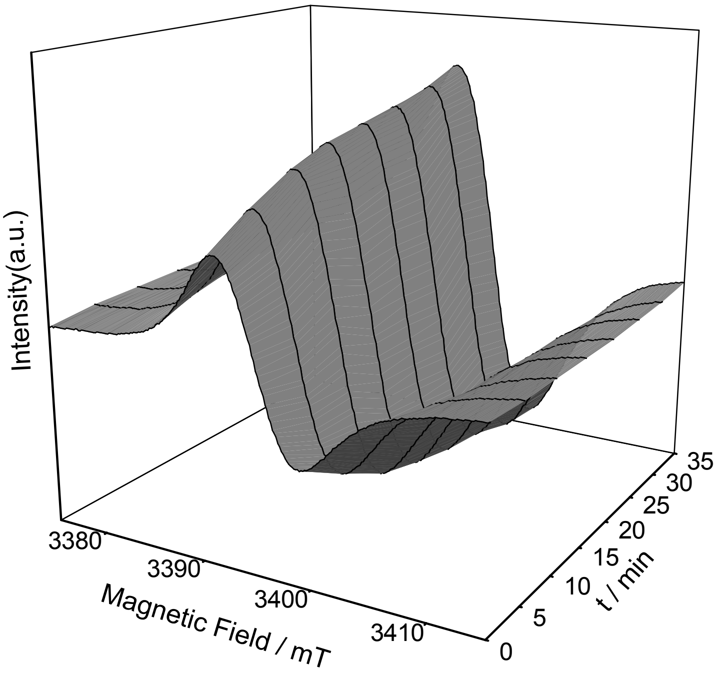

Figure 3.5 ESR signal of doped poly(**I**) with I_2 vapor.

3.1.3.4 Spectroelectrochemical Behavior of Poly(I) and Poly(II)

The changes in electronic transitions caused by varying the potential between redox states of the conjugated polymers can be investigated, in situ, by combining a suitable electroanalytical technique with a spectroscopic technique.

This combined technique is known as spectroelectrochemistry, SPEL, and gives information not only about the electronic transitions but also about the electronic band gap (E_g). In order to get such information about poly(**I**) and poly(**II**), related polymer films were synthesized on ITO working electrode at 1.9 V vs. SCE in 0.1 M TBAPF6/CH_3CN solution utilizing CPE. The polymer coated ITO was placed into the UV cell containing monomer-free electrolytic solution. Spectroelectrochemical behavior of polymer films were investigated by increasing the applied potential, by 100 mV increments, until the polymer reaches its fully oxidized and neutral forms. These redox states were reached when the polymer absorption band stops changing with increasing/decreasing applied potential.

The changes in the electronic absorption spectrum of poly(**I**) and poly(**II**), observed during a positive scan from 0.0 to 1.5 V for poly(**I**) and 0.0 to 1.1 V for poly(**II**) vs. Ag-wire, are recorded and the results are depicted in Figure 3.5. As can be seen from Figure 3.6(a) and Figure 3.6(b), the poly(**I**) and the poly(**II**) films show decreasing $\pi\rightarrow\pi^*$ transition band at 420 nm and 430 nm, respectively. The new bands centered at around 730 nm for both of the polymers start to increase during the positive scan. The formation of the new bands indicates the formation of polarons. In the potential range from 1.2 to 1.5 V, a broad bipolaron absorption band was also observed beyond 900 nm. It is important to note that, the oxidized film immediately reverts to the neutral state after stopping the applied potential. This observation is consistent with the results obtained during in situ ESR studies and related to the stability of polymer films in their neutral states.

In addition, from the commencement on the low energy end of the $\pi\rightarrow\pi^*$ transition band, in the neutral state, the band gap values of 2.11 eV and 2.09 eV were found for poly(**I**) and poly(**II**), respectively. These values are slightly higher than that of PTh (E_g = 2.00 eV) (see Figure 3.7).

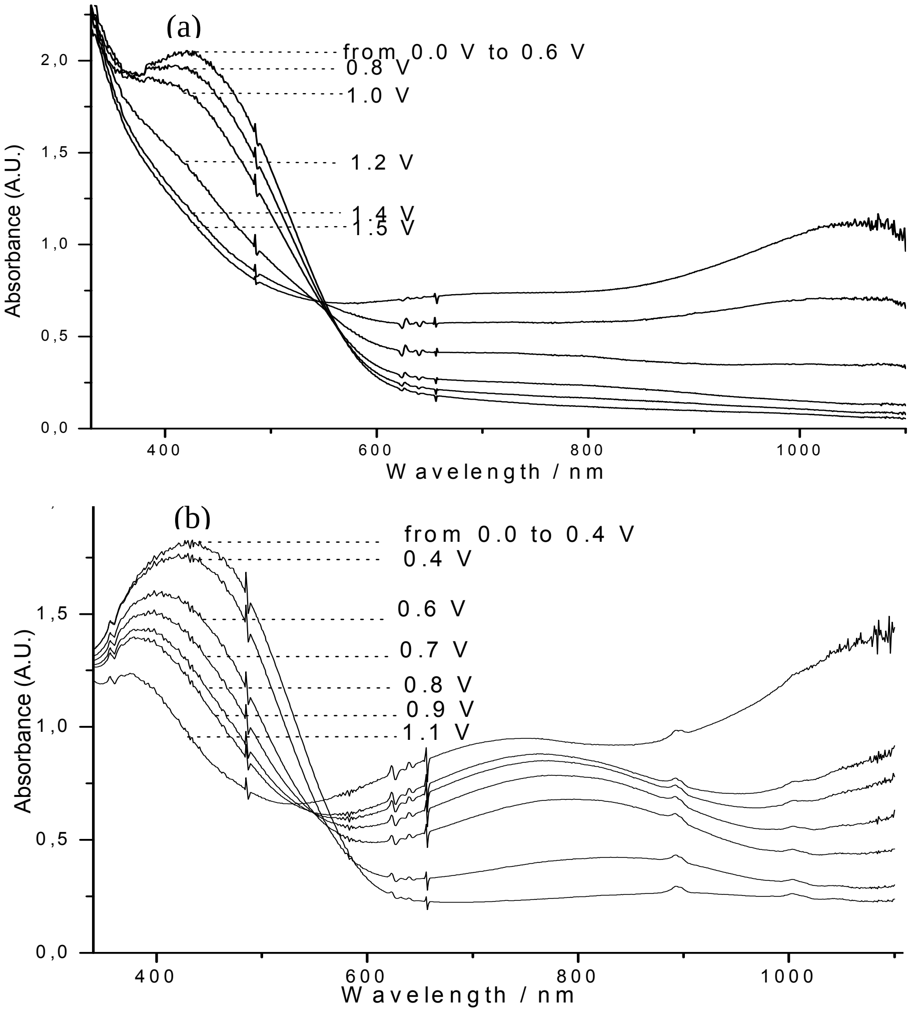

Figure 3.6 SPEL behavior of (a) poly(**I**) and (b) poly(**II**) in monomer-free electrolytic solution containing 0.1 M TBAPF6 dissolved in CH_3CN.

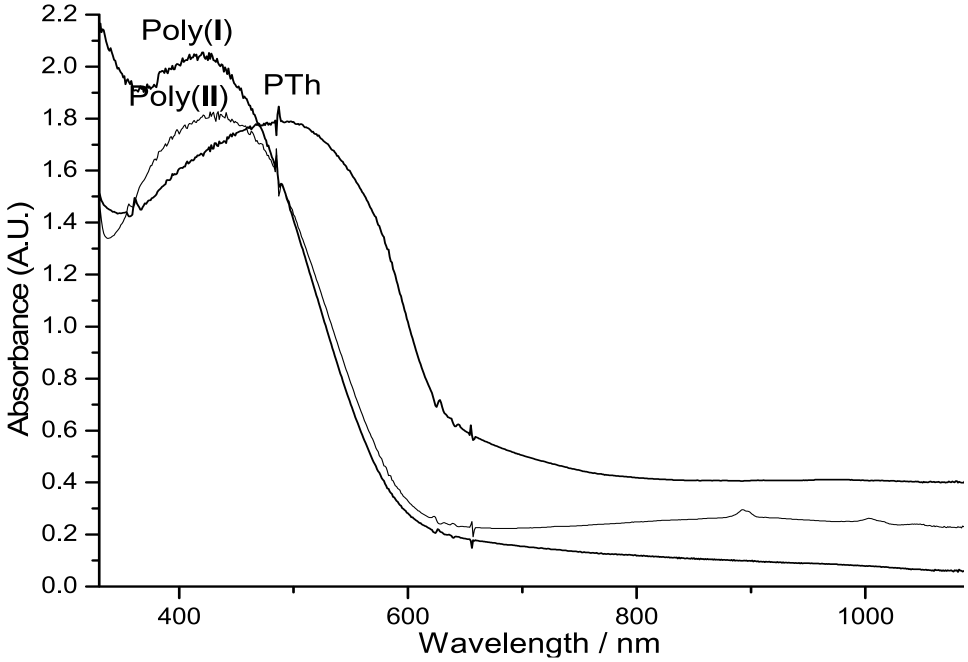

Figure 3.7 UV spectra of poly(**I**), poly(**II**), and PTh in their neutral state.

3.2 Polymers of ortho Substituted ANI Derivatives Linked by Polyether Bridges

3.2.1 Synthesis and Characterization of 2,2'-[ethane-1,2-diylbis(oxyethane-2,1-diyloxy)]dianiline (MIII) and 2,2'-[oxybis(ethane-2,1-diyloxyethane-2,1-diyloxy)]dianiline (MIV)

The syntheses of 2,2'-[ethane-1,2-diylbis(oxyethane-2,1-diyloxy)]dianiline (**MIII**) and 2,2'-[oxybis(ethane-2,1-diyloxyethane-2,1-diyloxy)]dianiline (**MIV**) were achieved according to the procedure described in the literature [106].

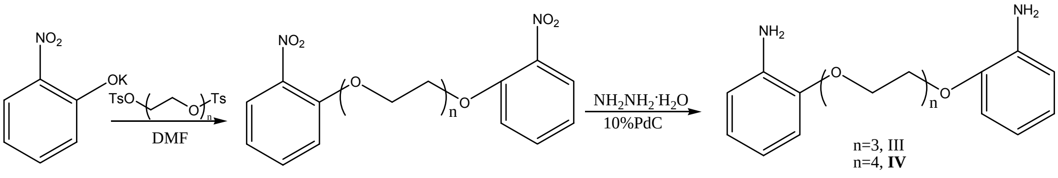

Figure 3.8 Synthesis of **MIII** and **MIV**.

3.2.1.1 Characterization of MIII by NMR Spectroscopy

^{1}H NMR (400 MHz, CDCl3) δ/ppm: 3.77 (s,4H) ppm, 3.89 (t, 4H, J = 4.65 Hz) ppm, 4.19 (t, 4H, J = 4.63 Hz) ppm, 4.36 (bs, 4H) ppm, 6.77-6.88 (m, 8H) ppm.

^{13}C NMR 100 MHz (CDCl3) δ/ppm: 146.35, 137.23, 121.93, 118.26, 115.35, 113.16, 70.79, 69.89, 68.48.

3.2.1.2 Characterization of MIV by NMR Spectroscopy

^{1}H NMR (400 MHz in $CDCl_3$) δ/ppm: 3.69-3.74 (m, 8H) ppm, 3.8 (bs, 4H), 3.86 (t, 4H, J = 4.70 Hz) ppm, 4.16 (t, 4H, J = 4.69Hz) ppm, 6.63-6.83 (m, 8H).

^{13}C NMR 100 MHz ($CDCl_3$) δ/ppm: 146.42, 136.93, 121.88, 118.40, 115.48, 113.12, 70.76, 70.65, 69.82, 68.43.

3.2.2 Voltammetry Studies of MIII and MIV

Prior to electrochemical polymerization, the electrochemical behavior of the monomers, **MIII** and **MIV**, were investigated utilizing CV. Cyclic voltammograms of the monomers were recorded in 3.0 M H_2SO_4*(*aq*)* at room temperature and measured peak potentials are tabulated in Table 3.2. As can be seen from the table, the length of polyether bridge has no significant effect on the anodic peak potential values of the monomers. During repetitive cycling between 0.0 and 1.0 V versus Ag/AgCl a new reversible peak starts to intensify indicating the formation of an electroactive polymer film on the electrode surface (Figure 3.9(B)). The electrochemical response of the polymer films, Poly(**III**) and Poly(**IV**), synthesized from **MIII** and **MIV**, respectively, in the monomer-free environment are also shown in Figure 3.9(C).

Table 3.2 CV data for **MIII**, **MIV**, poly(**III**), and poly(**IV**) vs. SCE

Monomers	Monomer		Polymer	
	E_{pa}(V)		E_{pa}(V)	E_{pc}(V)
MIII	0.97	Poly(**III**)	0.48	0.42
MIV	0.98	Poly(**IV**)	0.47	0.43

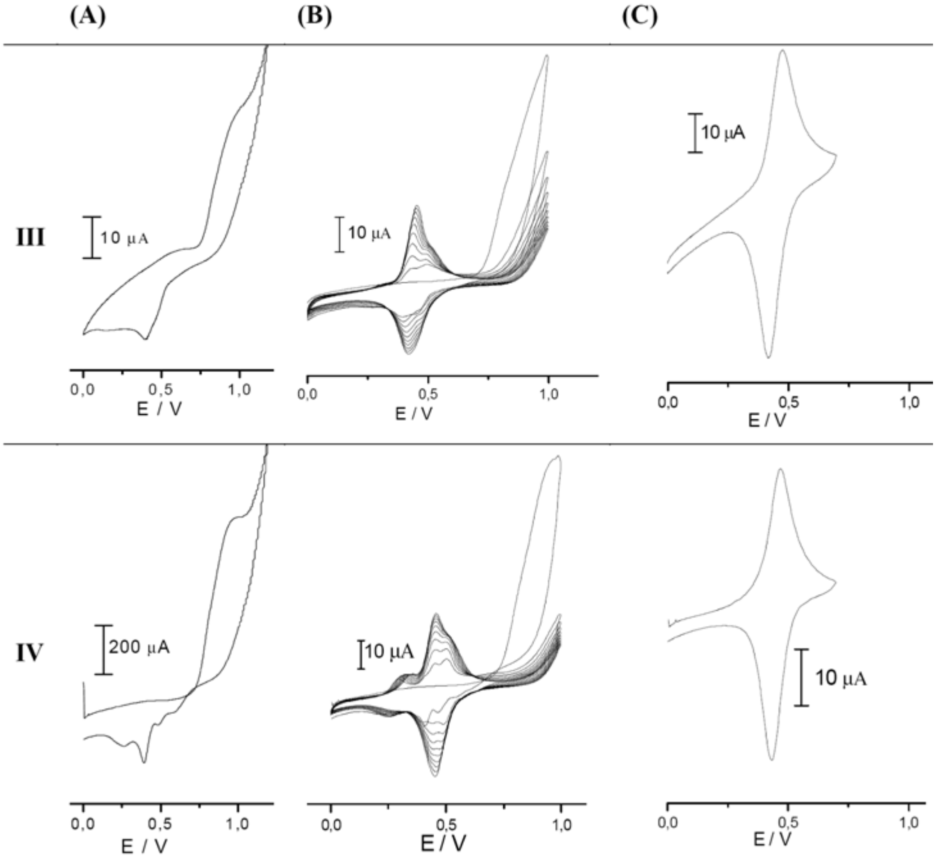

Figure 3.9 CV traces. (A) 0.1 M **MIII** and **MIV**. (B) Repetitive cycling of **MIII** and MIV, and (C) Poly(**III**) and Poly(**IV**), respectively, in monomer-free solution of 3.0 M H_2SO_4(aq); voltage scan rate = 200 mVs^{-1} (vs. Ag/AgCl).

3.2.3 Polymer Synthesis and Characterization

Although electrochemical polymerizations of **MIII** and **MIV** were investigated in organic and aqueous solutions, synthesis of freestanding polymer films could only be achieved in water with high acid concentration (i.e. 3.0 M H_2SO_4(aq)). Therefore, CV and CPE at 1.0 V *versus* Ag/AgCl techniques were applied for the polymerization of monomers in 3.0 M H_2SO_4(aq). Cyclic voltammograms recorded during the polymerization of **MIII** on ITO electrode and the changes in the electronic absorption spectrum of the monomer recorded during CPE are shown in Figure 3.10. As seen from Figure 3.10(b), three new absorption bands develop at around 370, 510 and 825 nm, during the in situ polymerization of **MIII**.

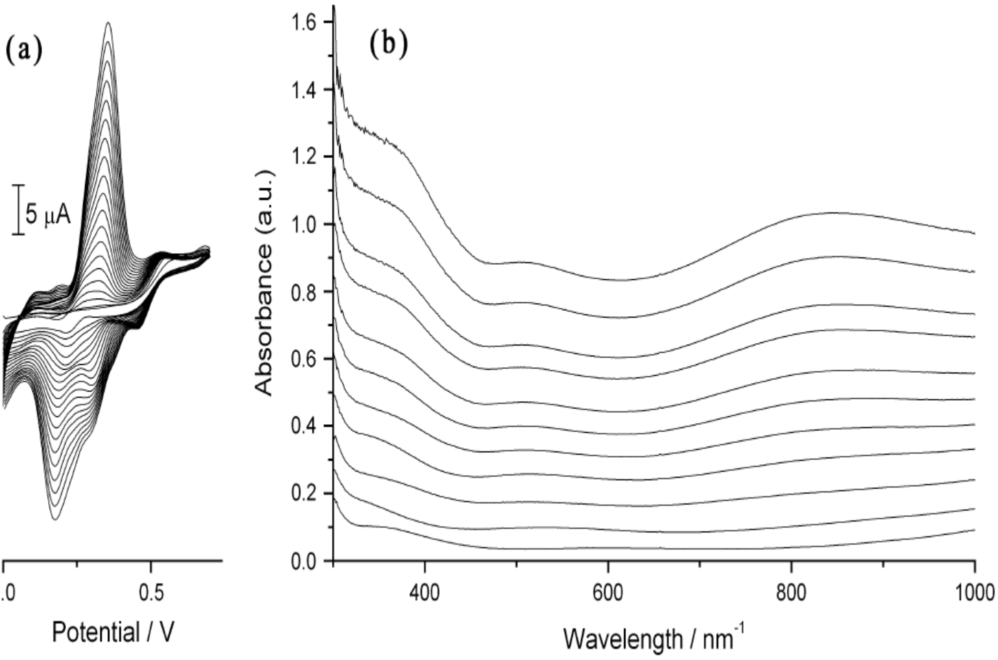

Figure 3.10 (a) Cyclic voltammogram of **MIII** during polymerization on ITO (voltage scan rate = 50 mVs^{-1}, versus Ag wire); (b) in situ polymerization of **MIII** during CPE (at 1.0 V versus Ag/AgCl, runs represent 5 s interval).

3.2.3.1 Electrochemical Behavior of Poly(III) and Poly(IV)

In order to investigate the effect of voltage scan rate, working electrodes coated with related polymers, (poly(**III**) and poly(**IV**)), were cycled between oxidized and reduced states at various scan rates in monomer-free aqueous solution containing 3.0 M H_2SO_4. The results are depicted in Figure 3.11. The peak current values were found to increase linearly with increasing scan rate indicating that the redox process is non-diffusional and the electroactive polymer is well adhered to the WE surface.

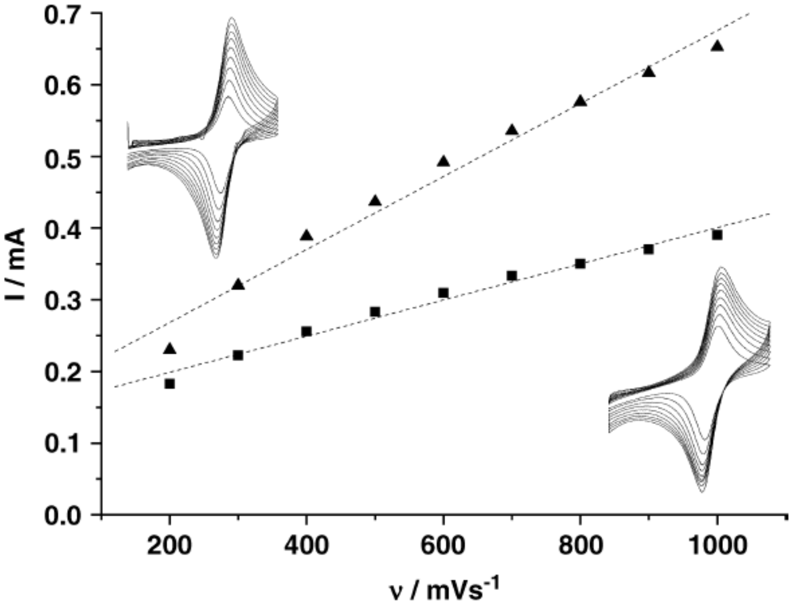

Figure 3.11 Anodic peak height (I_{pa}) versus voltage scan rate (v): (■) Poly(**III**) (r^2 = 0.99); (▲) Poly(**IV**) (r^2 = 0.99).

In order to get information about polymer stability, the polymer film was cycled 1000 times between its redox potentials. The results depicted in Figure 3.12 reveal that the polymer film does not lose its electroactive properties completely. After 1000 cycles the polymer gave a redox response retaining 70% of its electroactivity.

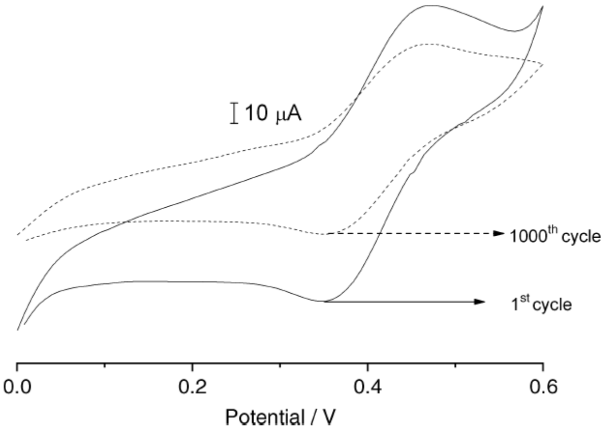

Figure 3.12 Cyclic voltammogram of poly(**III**) as a function of repeated scans (500 mVs^{-1}).

3.2.3.2 FT-IR Analysis

Figure 3.13 shows the FTIR spectra of **MIII** and its polymers obtained by electrochemical and chemical polymerizations. Comparison with FTIR spectrum of the monomer reveals that the triplet at about 3300 cm^{-1} becomes a broad band at about 3250 cm^{-1} which indicates that electrochemical polymerization occurs via $-NH_2$ groups. The bands at 1505 and 1576 cm^{-1} correspond to quinoid and benzenoid structures of polymer film. In addition, bands at 1245 and 1195 cm^{-1} can be assigned to vibrations of –C–N bonds in quinoid and benzenoid rings.

Also, the presence of polyether bridges in the polymer film is confirmed by the bands at 2866 and 1105 cm^{-1} which are attributed to aliphatic –C–H stretching and –C–O–C stretching, respectively. The bands at about 751 and 829 cm^{-1} are associated with *ortho*- and *para*- substitution in the polymer backbone. Also, the FTIR spectrum of Poly(**III**) obtained via chemical oxidation (Figure 3.13(c)) is almost same as that obtained via CPE. By considering the obtained results, the proposed structure of poly(**III**) is depicted in Figure 3.14.

The results achieved for the polymerization of **MIII** are also valid for the poly(**IV**). Common bands, 3260 cm^{-1} for $-NH_2$ groups, 1590 and 1490 cm^{-1} for benzenoid and quinoid structures, 1107 cm^{-1} for C-O-C stretching and 755 and 828 cm^{-1} for *ortho* and *para* substitutions of backbone can be seen from Figure 3.15(a)

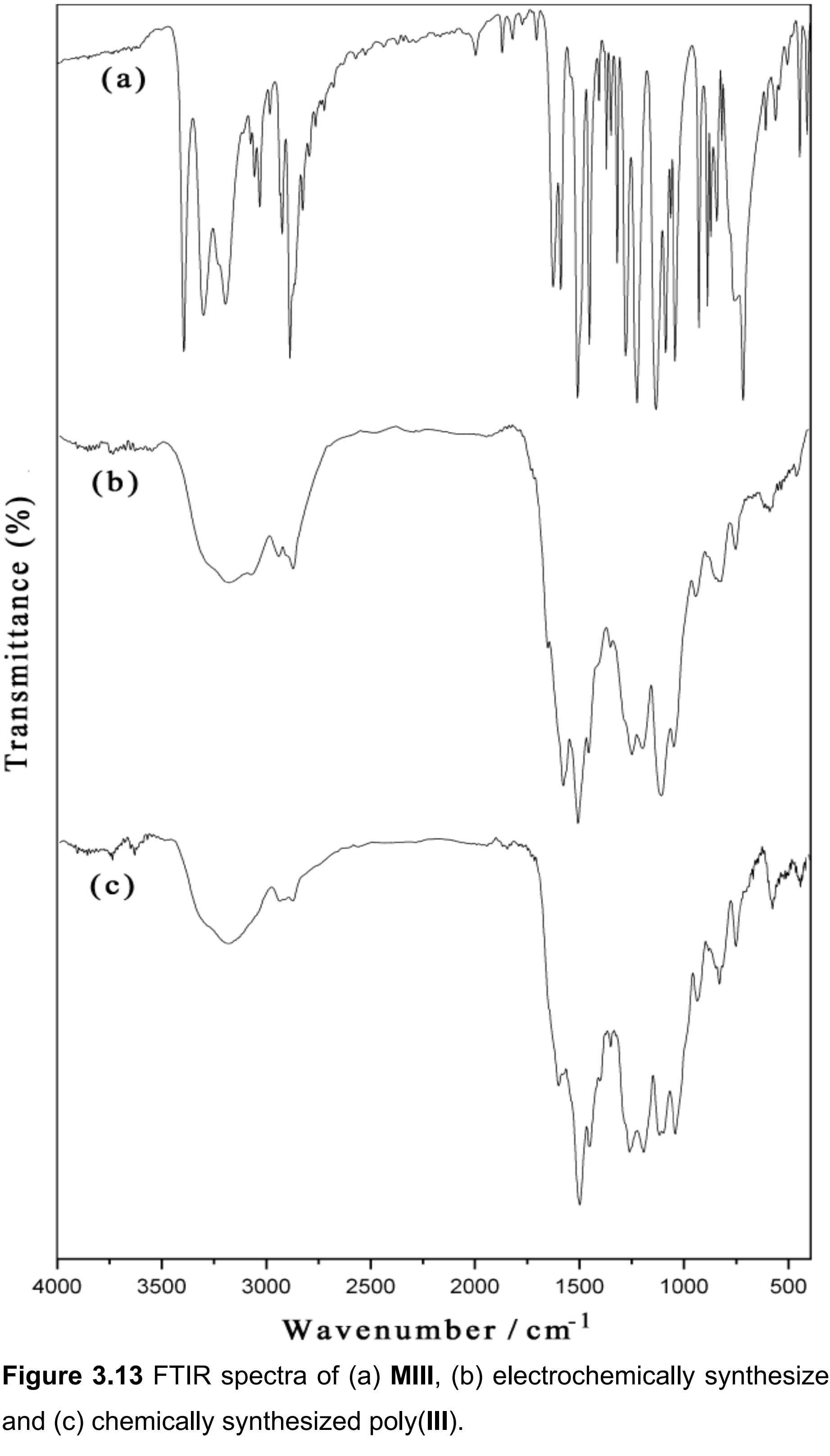

Figure 3.13 FTIR spectra of (a) **MIII**, (b) electrochemically synthesized poly(**III**) and (c) chemically synthesized poly(**III**).

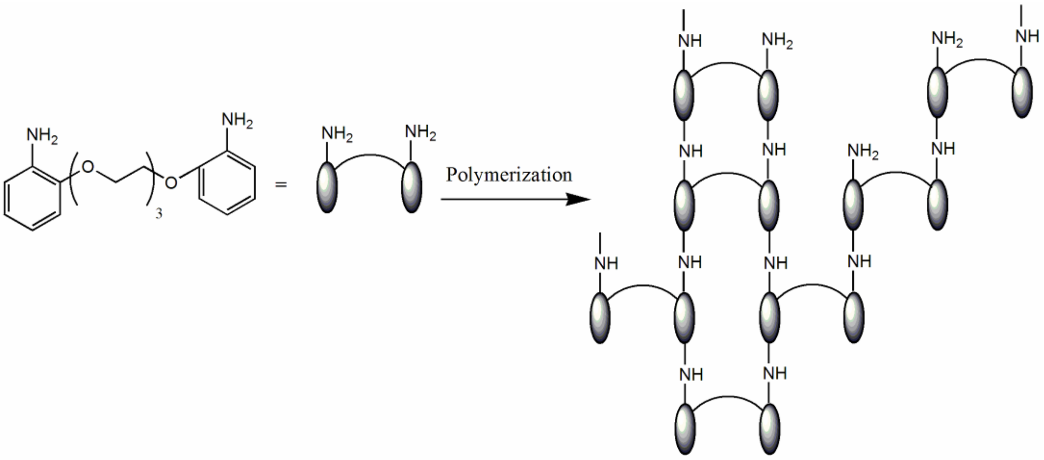

Figure 3.14 Proposed structure for electrochemically and chemically synthesized Poly(**III**).

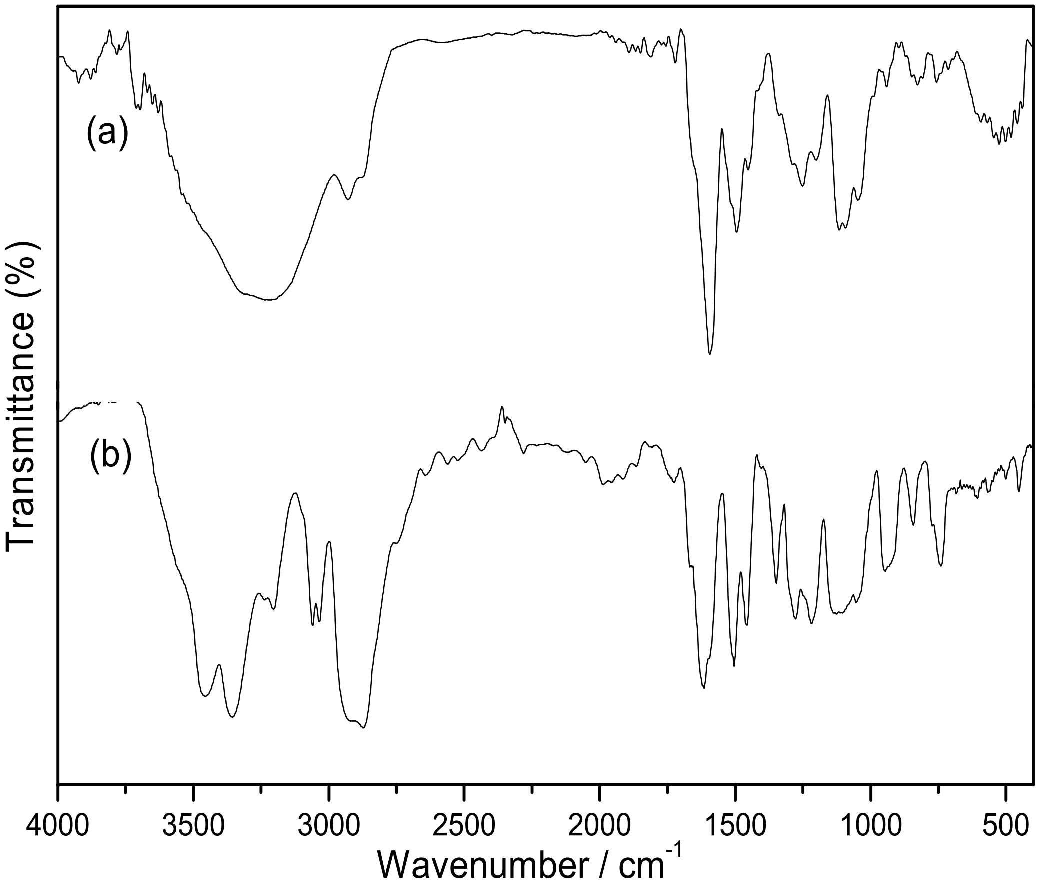

Figure 3.15 FTIR spectra of (a) electrochemically polymerized Poly(**IV**), (b) **MIV**.

3.2.3.3 Thermal Gravimetric Analysis of Poly(III)

The thermal behavior of Poly(**III**) is illustrated along with the TGA curves in Figure 3.16 The first weight loss (80-150 °C) indicates the loss of water molecules in the polymer matrix. The second weight loss occurs at around 300 °C which may be attributed to loss of dopant. The last weight loss is observed at around 500 °C and then complete degradation occurred.

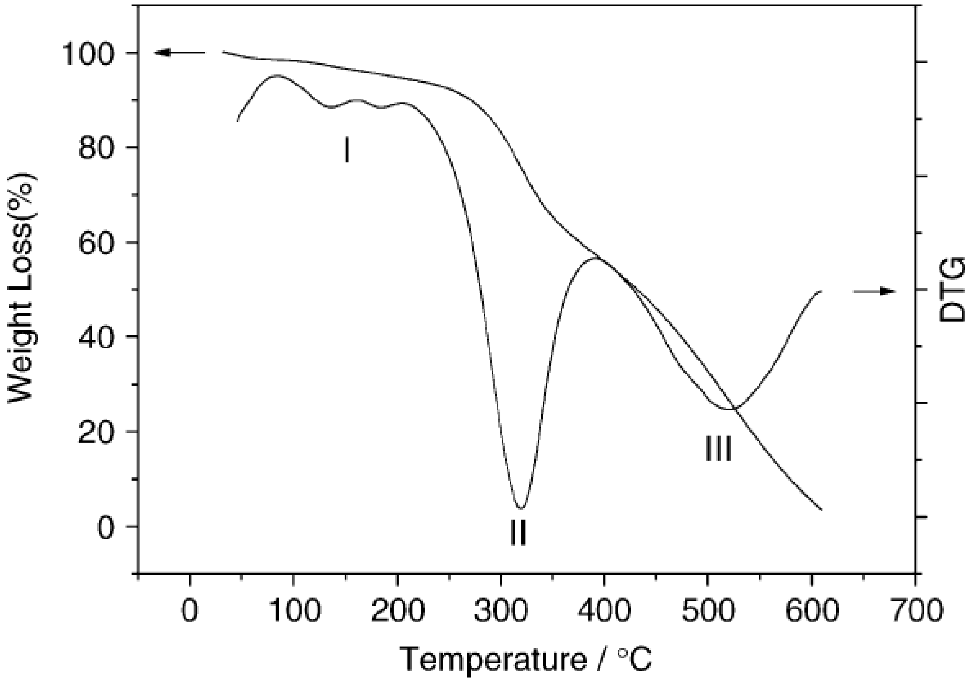

Figure 3.16 TGA thermogram of Poly(**III**) (heating rate = 10 °C min^{-1}).

3.2.3.4 Spectroelectrochemical Behavior of Poly(III) and Poly(IV)

In order to investigate the SPEL behavior of Poly(**III**), the polymer film was deposited on ITO electrode using CV in 3.0 M H_2SO_4 solution. The changes in the electronic absorption spectrum of the polymer were monitored at various applied potentials in monomer-free electrolytic solution and the results are shown in Figure 3.17.

The electronic absorption spectrum of neutral Poly(**III**) has two absorption bands at about 325 and 430 nm (Figure 3.17b)). The former absorption band is attributed to π→π* transitions and the latter to radical cation intermediate [107]. The electronic band gap of the polymer can be estimated from the onset of the π→π* transition in the neutral form. From its commencement on the low-energy end, the band gap was found to be 3.07 eV. This value is consistent with the very low conductivity of the polymer film. It was reported that alkyl substitution increases the torsion angle between phenyl rings in the polymer backbone and therefore decreases the degree of orbital overlap between π-electrons in the phenyl rings and the lone electron pairs of nitrogen [108,109,110,111] This causes a decrease in length of conjugation and conductivity which might be the reason for the very low conductivity of poly(**III**) and poly(**IV**). During the anodic scan, the band at 325 nm decreases and the 430 nm band shifts to lower wavelengths. As the applied potential increases, a new band at about 520 nm intensifies indicating the formation of polarons in the polymer film. The response of Poly(**IV**) was similar to Poly(**III**) in the same potential range.

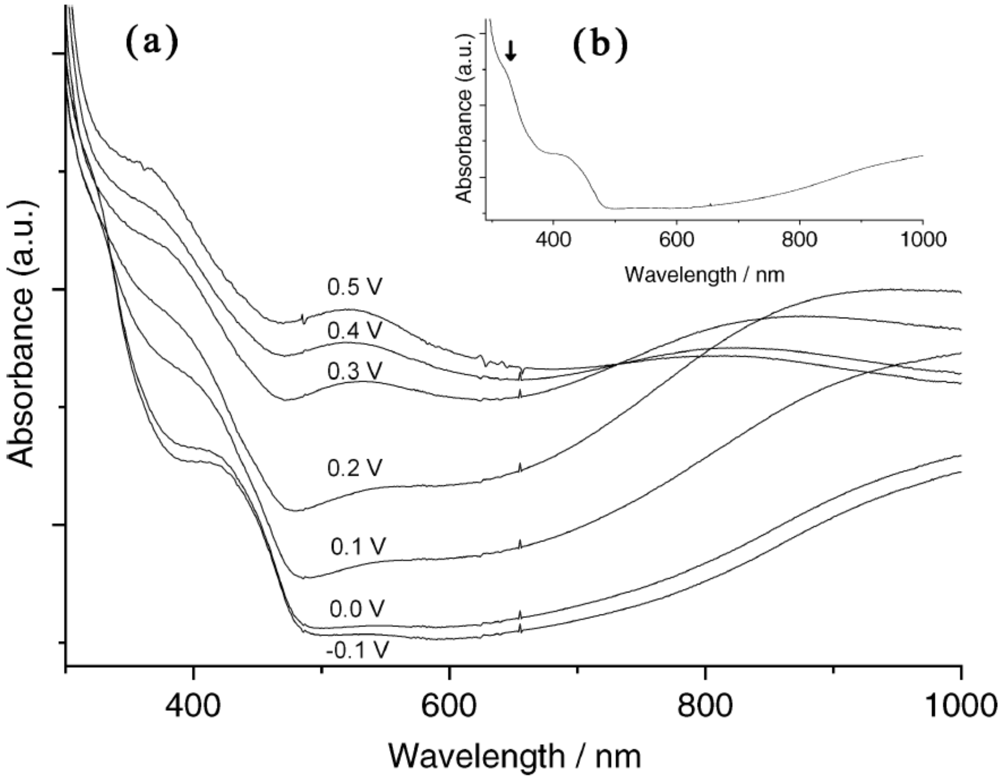

Figure 3.17 (a) SPEL behavior of Poly(**III**) in monomer-free aqueous solution of 3.0 M H_2SO_4. (b) Spectrum of neutral form of Poly(**III**).

3.3 Copolymers of MIII and MIV with ANI

Since poly(**III**) and poly(**IV**) (synthesized from **MIII** and **MIV** respectively) were found to have very low conductivity, we have also investigated copolymerization of both monomers with ANI to obtain copolymers with reasonable electrical conductivities. At least three different **MIII**/ANI (or **MIV**/ANI) feed ratios were used for this purpose.

3.3.1 Voltammetric Studies of Mixture of MIII and ANI

In addition to the voltammetric data of **MIII**, which was given in section 3.2.2, we have studied the electrochemical behavior **MIII/**ANI mixture with various compositions (Figure 3.18). As seen from the following cyclic voltammogram the oxidation potential of **MIII** shifted to more positive potentials with increasing amount of **MIII** in the co-monomer mixture. Before the detailed investigation of electrochemical behavior of **MIII**/ANI mixtures, we have also investigated the redox behavior of ANI in 3.0 M H_2SO_4 solution and CV recorded under these conditions is depicted in Figure 3.19. It is found that repetitive cycling of ANI solution in presence of high acid concentration also results in polymer formation. After 25 cycles the film was washed and immersed in monomer free solution. The cyclic voltammogram of the PANI film is given in Figure 3.20.

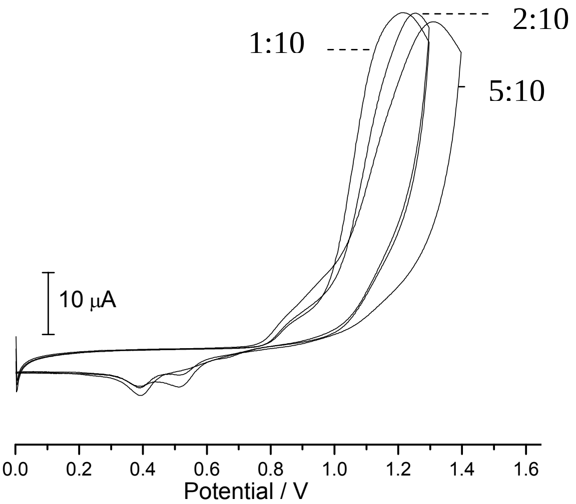

Figure 3.18 Cyclic voltammograms of different composition of (**MIII**/ANI); (1/10, 2/10, 5/10).

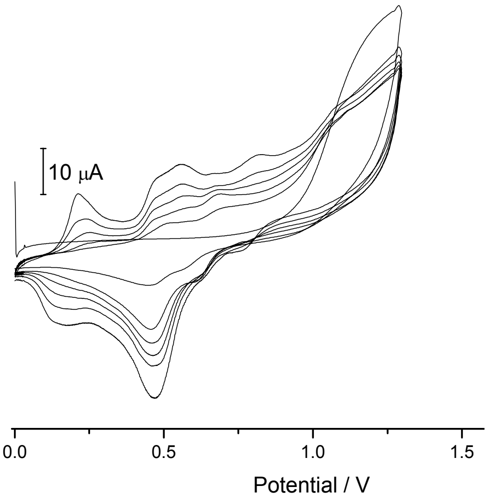

Figure 3.19 Repetitive cycles (1st, 5th, 10th, 20th, and 25th) of ANI during polymerization, recorded in 3.0 M H_2SO_4 solution.

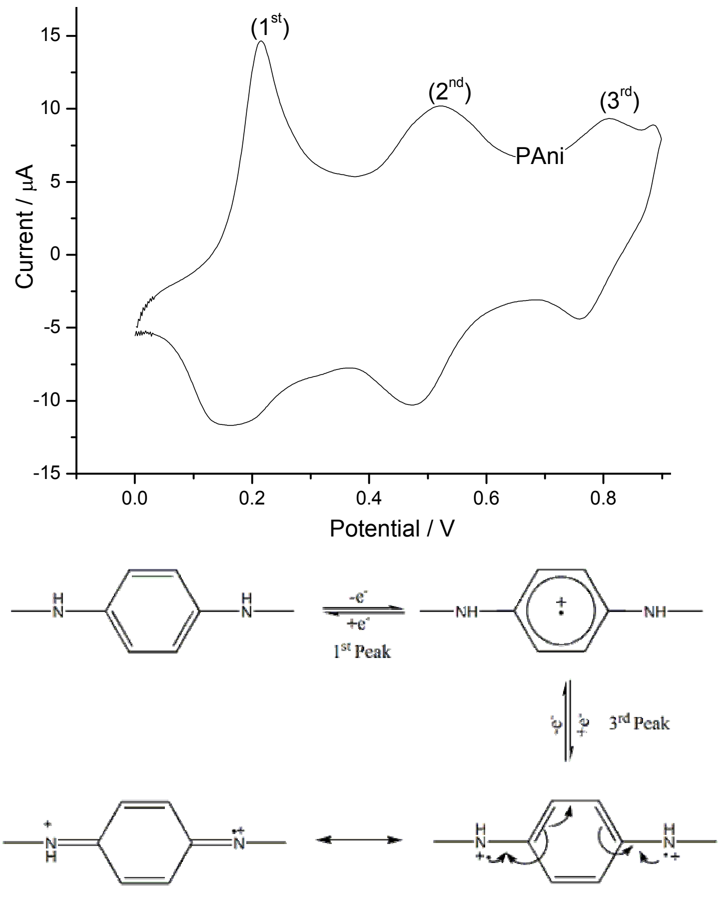

Figure 3.20 Cyclic voltammogram of PANI in 3.0 M H_2SO_4 solution.

As seen from the Figure 3.20, there are three reversible peaks at 216, 521 and 811 mV in the CV of PANI recorded in the monomer free electrolytic solution. The first redox couple (E_{pa}= 216 mV and E_{pc}= 168 mV) corresponds to leucoemeraldine-emeraldine salt transition. The second redox couple (E_{pa}= 521 mV and E_{pc}= 476 mV) corresponds to the quinone/hydroquinone transition, whose formation is possible because under acidic conditions the cation radical can be hydrolyzed to yield benzoquinone [112]. The third redox couple (E_{pa}= 811 mV and E_{pc}= 759 mV) reveals the transition between emeraldine salt and pernigraniline.

The cyclic voltammograms recorded for solutions with three different **MIII**/ANI compositions are given in Figure 3.21. Inspection of these CVs revealed that as the amount of **MIII** in the co-monomer mixture increases the increments between consecutive cycles increase (Figure 3.21 (a-c)).

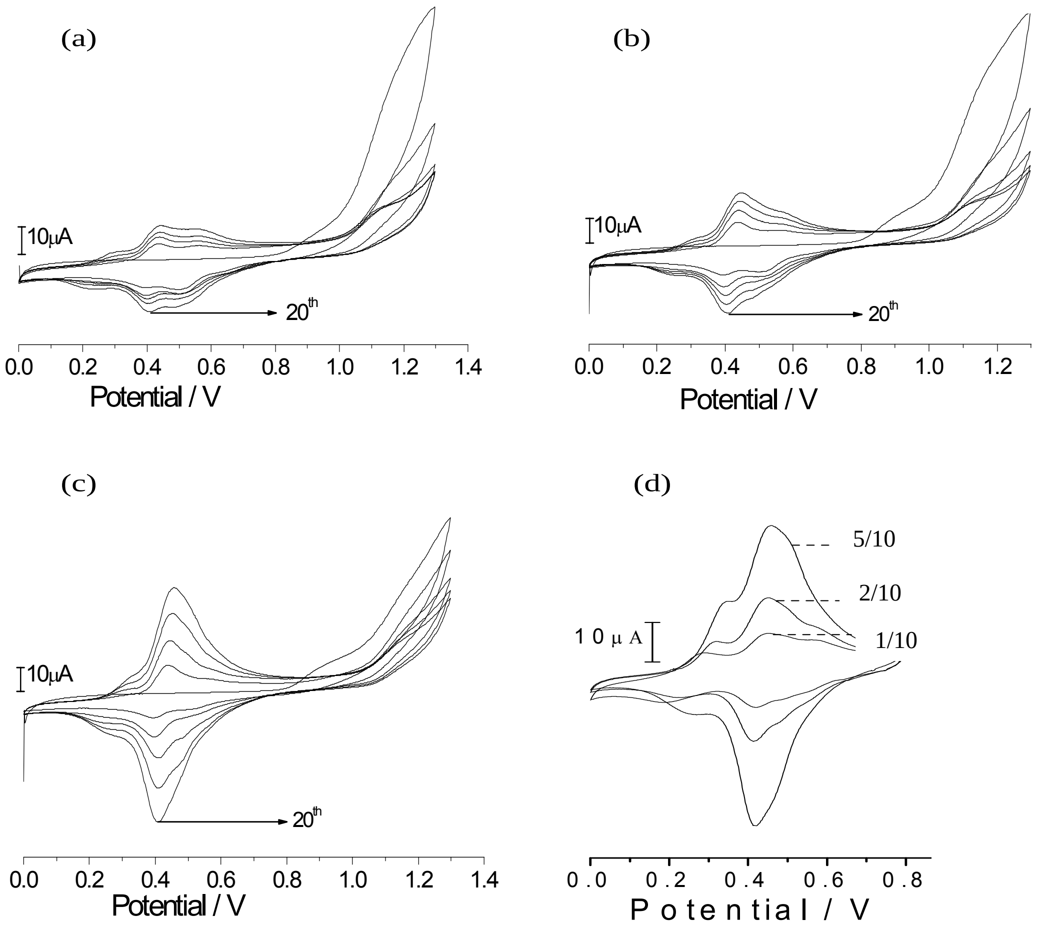

Figure 3.21 Repetitive cycles (1st, 5th, 10th, and 20th) of different monomer compositions (a) (**MIII**/ANI; 1/10), (b) (**MIII**/ANI; 2/10), (c) (**MIII**/ANI; 5/10), and (d) and polymer film obtained from the (**MIII**/ANI) mixtures.

3.3.2 Voltammetric Studies of Mixture of MIV and ANI

Copolymerization of **MIV** with ANI was also investigated utilizing CV. It is observed that as the amount of **MIV** increased in the co-monomer mixture, the growth rate was also increased for the copolymer formation (Figure 3.19). This behavior is not different than the one observed for **MIII**/ANI mixtures.

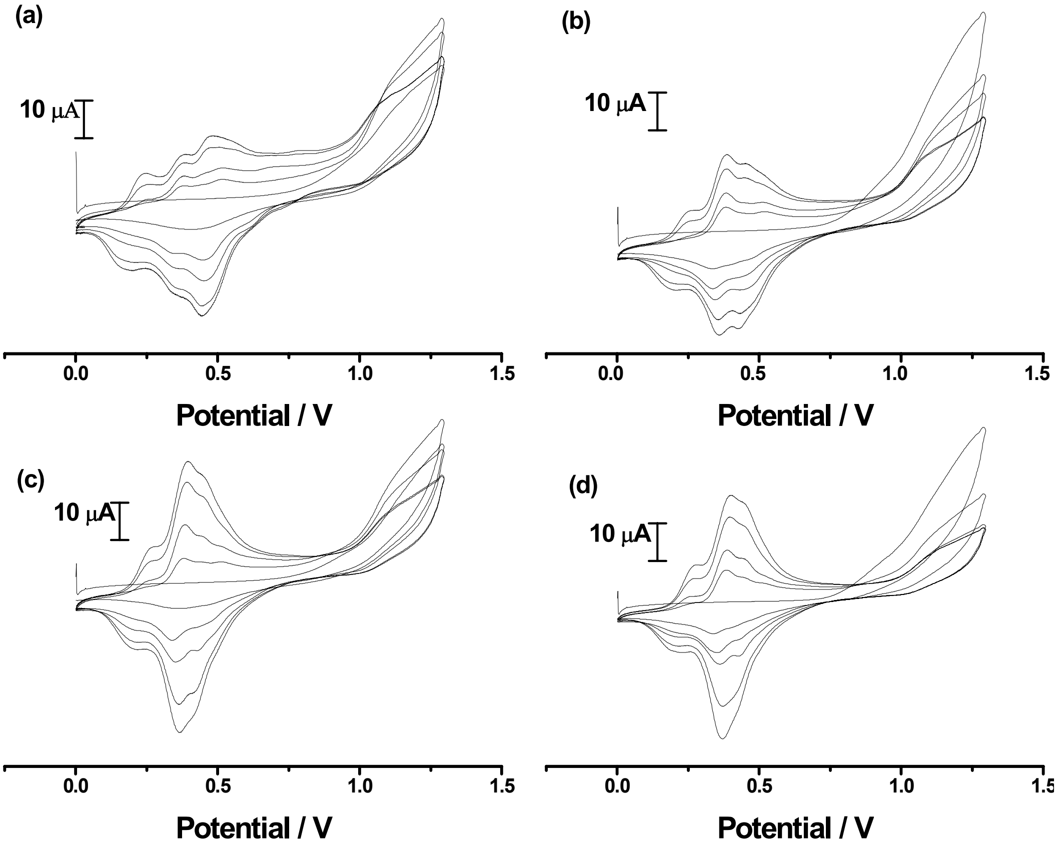

Figure 3.22 Repetitive cycles (1st, 5th, 10th, 20th, and 25th) of different monomer compositions; (a) (**MIV**/ANI; 10/1), (b) (**MIV**/ANI; 2/10), (c) (**MIV**/ANI; 4/10), and (d) (**MIV**/ANI; 6/10) in 3.0 M H_2SO_4.

CV of poly(**IV**) and PANI recorded in 3.0 M aqueous acidic solution are given in Figure 3.23 for comparison purposes. CVs of copolymers obtained from various co-monomer mixtures are also shown in the same figure. As it is seen from the figure, three redox couples decreased to one reversible signal in the CV of poly(**IV**). On the other hand, addition of ANI into the polymerization medium produces copolymers having two redox couples. The first redox couple that appears around 286 mV is most probably due to leucoemeraldine-emeraldine salt transition and this might be the evidence for explanation of conductivity of this copolymer.

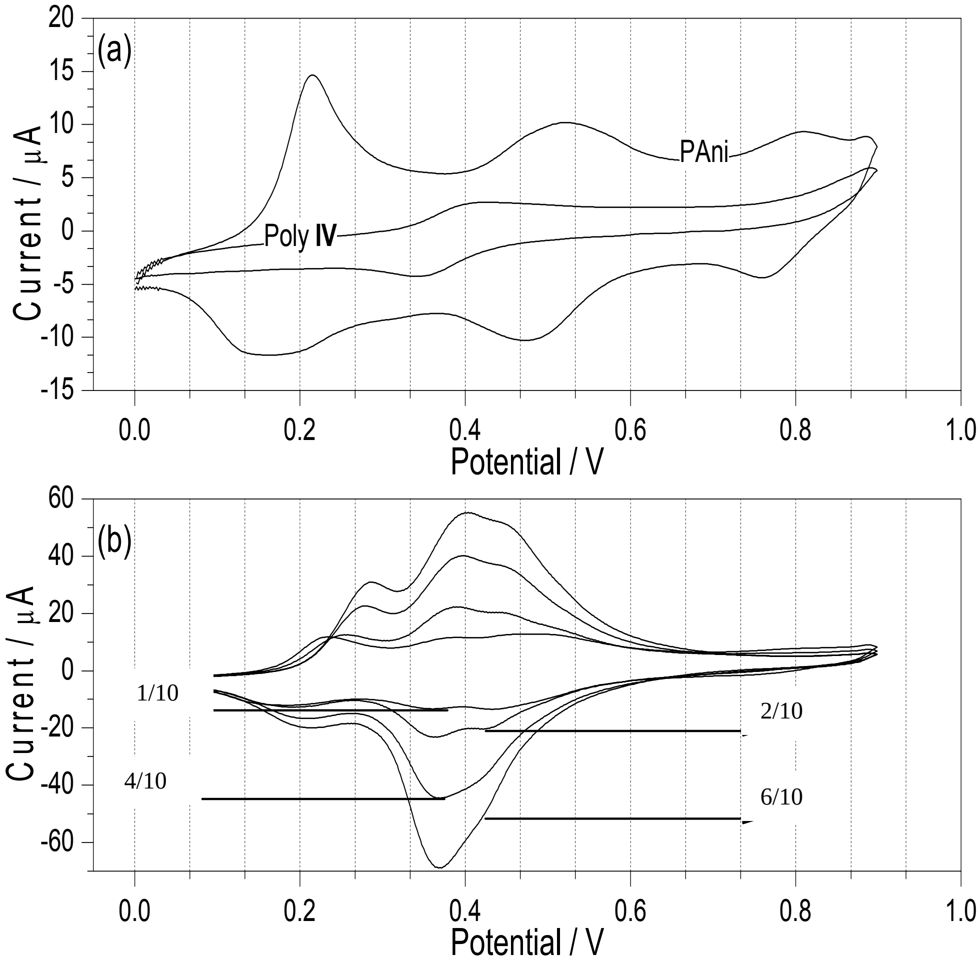

Figure 3.23 Cyclic voltammogram of (a) PANI and Poly(**IV**),(b) Poly(**IV**-co-ANI) of synthesized from different monomer compositions.

3.3.3 In situ Spectroelectrochemical Investigations on Copolymerization of MIII with ANI

Copolymerization of **MIII** with ANI was also investigated by in-situ recording the changes in the electronic absorption spectrum during constant potential electrolysis at 1.2 V vs Ag wire. The results are depicted in Figure 3.24. There are three absorption bands intensifying during CPE of M(III) at about 360, 510, and 830 nm. The lower wavelength band is most probably due to $\pi \rightarrow \pi^*$ transition of neutral molecules. The 510 nm band could be attributed to various mixed dimers arising from radical-radical coupling of different radical cations. The long wavelength that appears around 800 nm could indicate bipolaron.

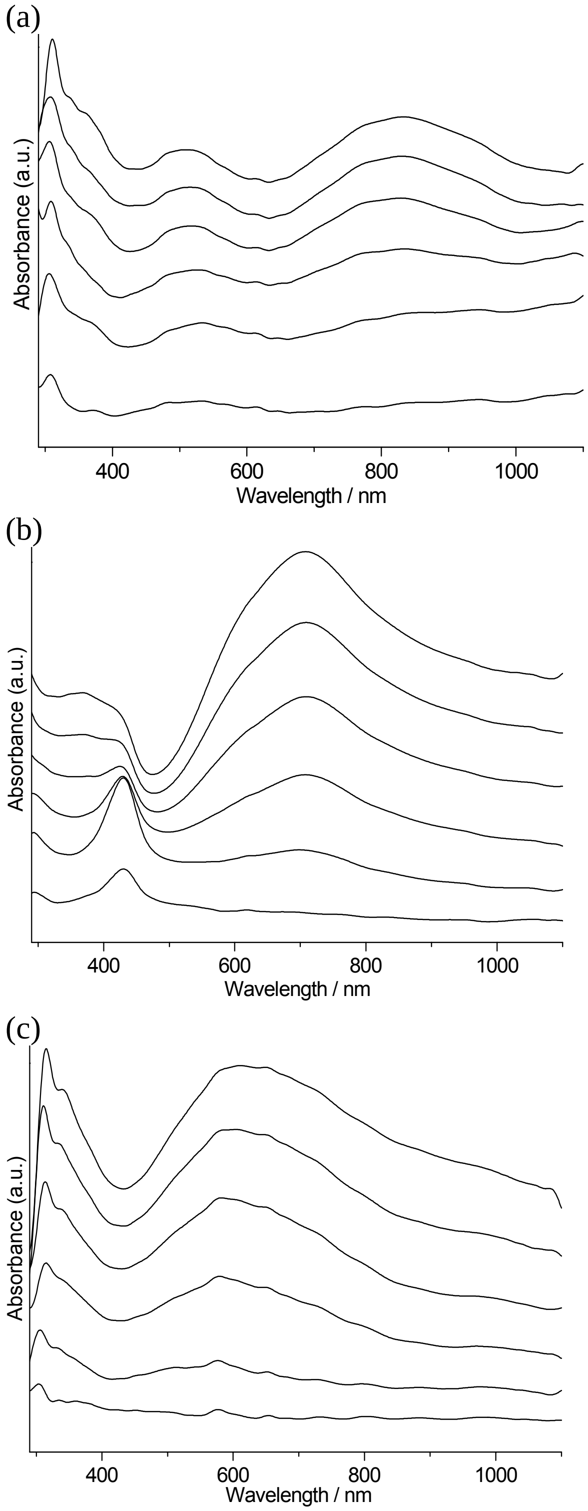

Figure 3.24. In situ UV-vis spectra of polymerization of (a) **MIII**, (b) ANI, and (c) **MIII**/ANI;2/10 monomer mixture.

The electronic absorption spectrum of ANI solution was also recorded during CPE (Figure 3. 24(b)). Formation of aniline cation radical at the beginning of reaction can be seen easily at 430 nm which becomes a shoulder as the reaction proceeds. The 360 nm and 710 nm bands could be attributed to $\pi \rightarrow \pi^*$ transition of neutral molecules, and N-phenyl-paraphenylenediamine dimer and its dication, respectively [113]. On the other hand, the spectra of M(**III**)/ANI mixture (Figure 3.24(c)) shows some different properties. Although the formation of radicals can not be observed as clearly as PANI formation, there is a broad band at 600 nm which might be due to formation of mixed radical cation dimer.

3.3.4 Structure and Morphology Analysis of Poly(III-co-ANI) by FT-IR, Scanning Electron Microscopy and Electron Spin Resonance

When the FTIR spectra of poly(**III**) and the copolymer film are compared, the similarity can be seen (Figure 3.25). The presence of aliphatic $-CH_2$ bands around 2860 cm^{-1}, and –C-O-C- bands around 1110 cm^{-1} in FTIR spectrum of copolymer is the evidence of the existence of polyether bridges in copolymer backbone. Furthermore, the peaks at about 748 and 810 cm^{-1} are associated with *ortho*- and *para*- substitution in the polymer backbone, indicating the presence of two adjacent hydrogen atoms.

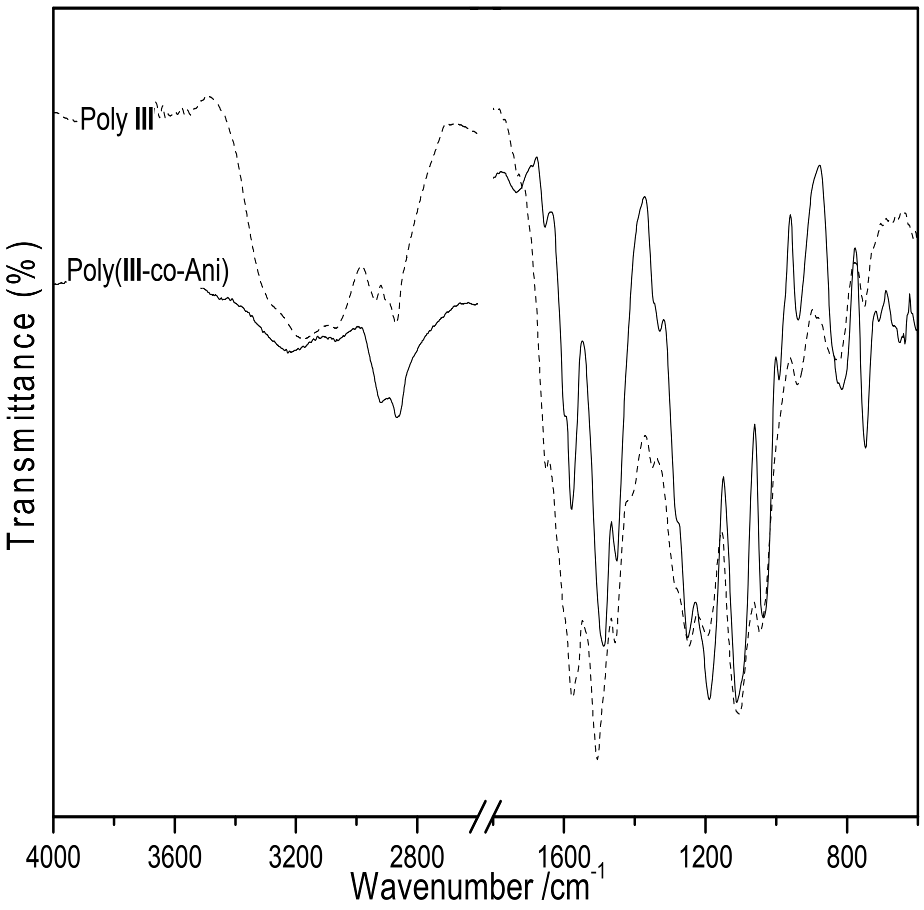

Figure 3.25 FTIR spectra of poly(**III**) (dashed line) and poly(**III**-co-ANI).

The micrographs of PANI, poly(III) and poly(III-co-ANI) are shown in Figure 3.26 (a-f).The surface of PANI obtained by potentiodynamic method contains fibrilar structure (Figure 3.26(d)), however, the poly(**III**) has highly smooth and uniform surface (figure 3.26(b)). On the other hand, the copolymer has different surface for both sides of the film (Figure 3.26(c, e).

The close inspection of PANI and copolymer micrographs reveals the copolymer formation. Instead of completely fibrilar structure of PANI (Figure 3.27 (a,b)), the copolymer has a varied morphology including both fibrils and relatively smoother surface. In addition to this, in copolymer film the penetrated and polymerized ANI may be also seen in Figure 3.27 (c, d).

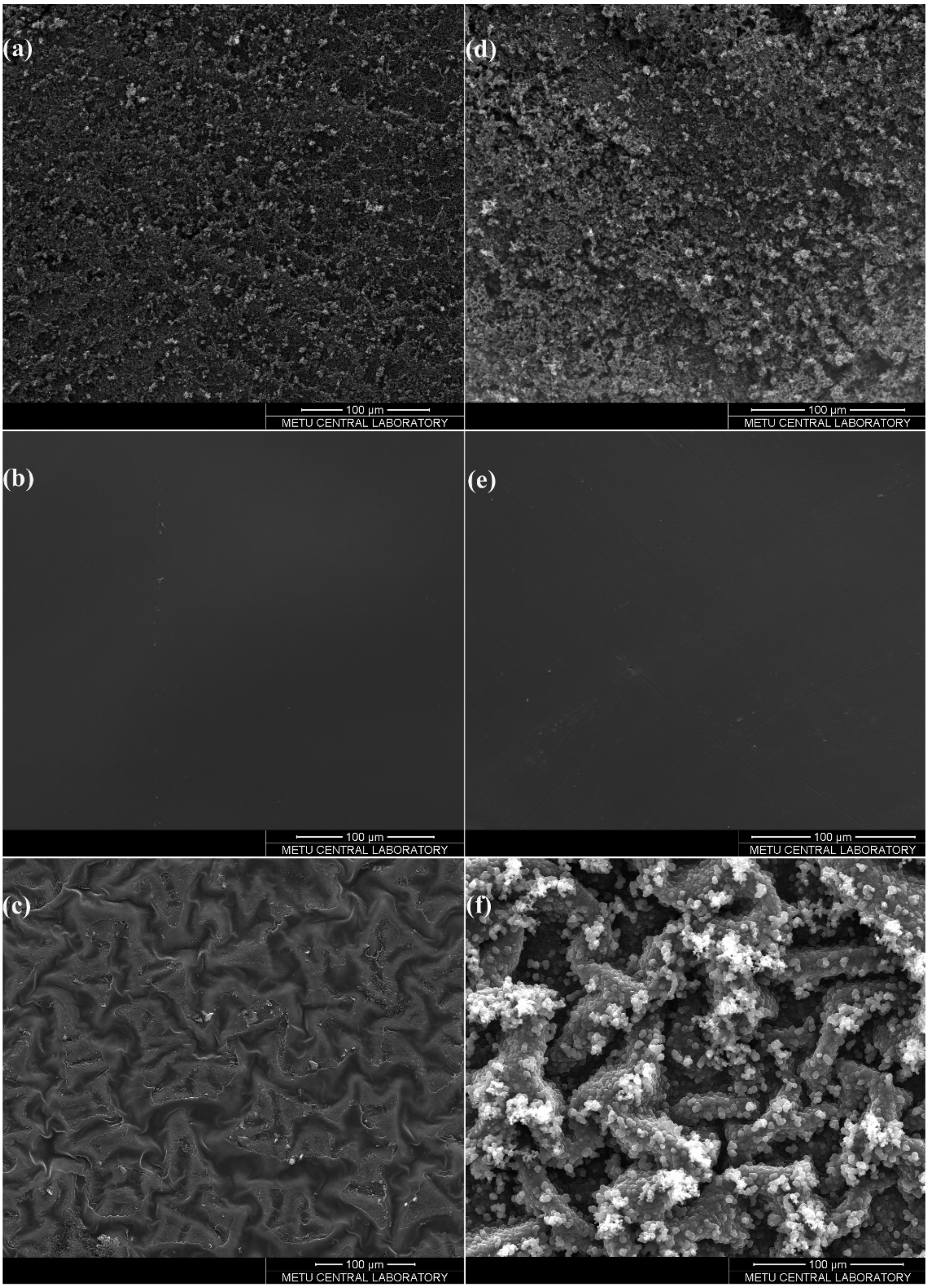

Figure 3.26 Scanning electron micrographs: electrode side of (a) PANI, (b) Poly(**III**), (c) Poly(**III**-co-ANI), and solution side of (d) PANI, (e) Poly(**III**), (f) Poly(**III**-co-ANI).

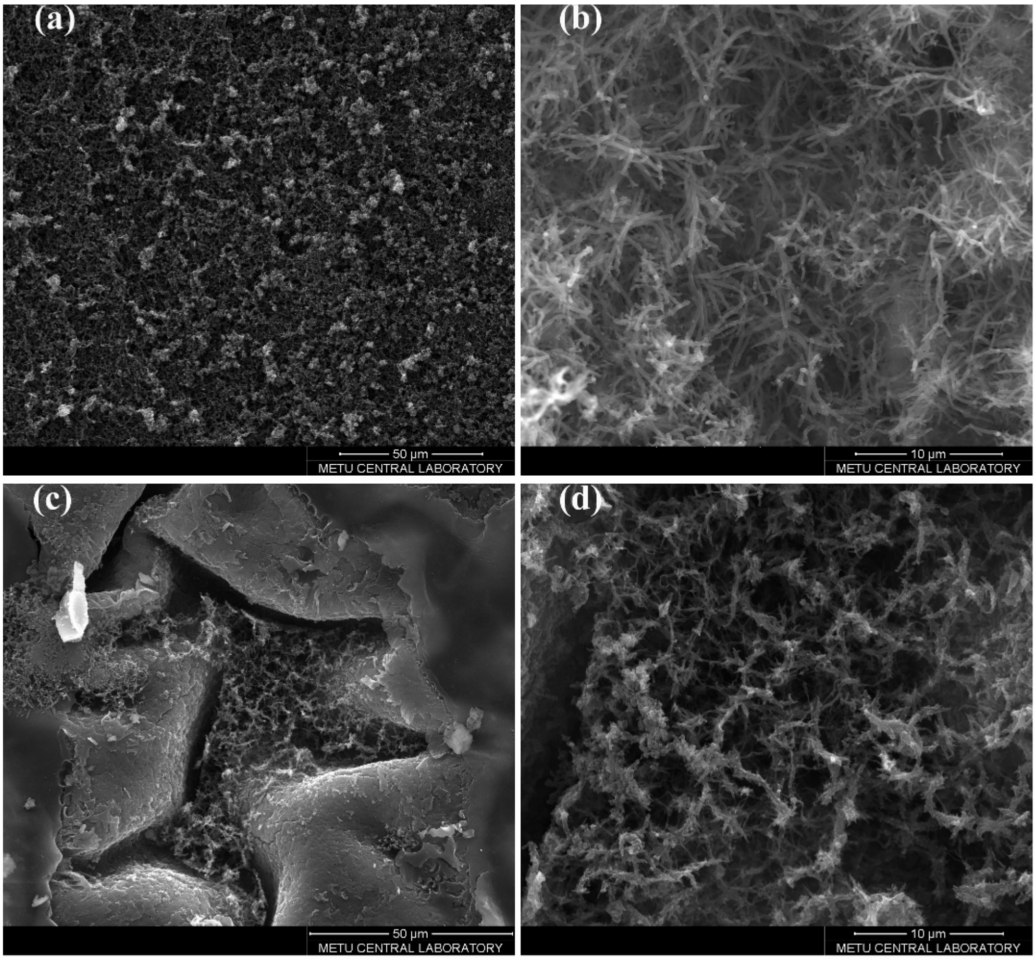

Figure 3.27 Electrode side scanning electron micrographs of: PANI (a) x1, (b) x5, Poly(**III**-co-ANI) (c) x1, (b) x5 (x1 and x5 are the relative magnifications).

In order to find further evidences for the copolymer formation we have also recorded ESR spectrum of homo and copolymers at room temperature. The results are shown in Figure 3.28. Although three spectra are similar in appearance, all in Dysonian shape, there are differences both in terms of line width and asymmetry ratio (A/B ratio). The line widths are found to be 2.2, 1.9 and 0.8 mT for PANI, Poly(**III**) and Poly(**III**-co-ANI), respectively. The asymmetry ratio (A/B ratio) also varies from sample to sample which is thought to be related to the conductivity of the polymer. Increasing A/B indicates an increase in conductivity. Thus, the increase of A/B from 1.5 to 3.1 due to copolymerization is not only a further evidence for copolymer formation but also indicates enhancement of conductivity.

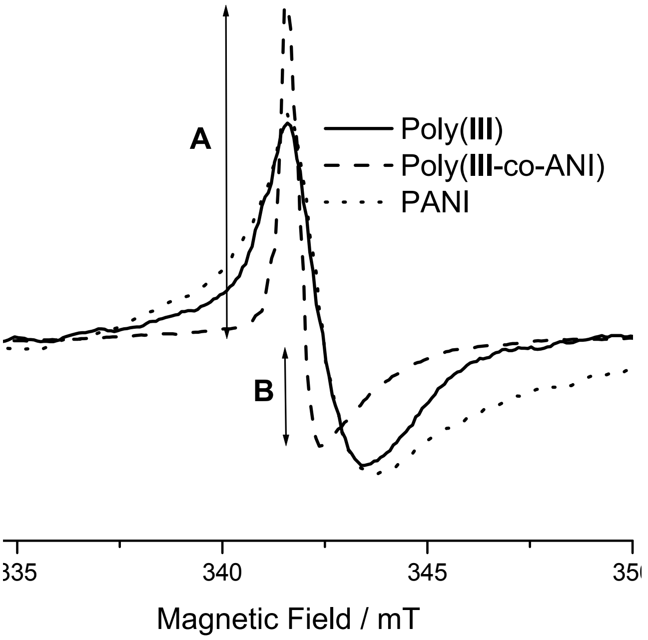

Figure 3.28 ESR spectra of PANI, Poly(III) and Poly(III-co-ANI) recorded at room temperature, field setting 3361 G and microwave power 5 mW.

3.3.5 SPEL Behavior

The UV-vis spectra of PANI can be seen in Figure 3.29(a) The absorption around 295 nm is due to the π→π* transition of benzenoid rings of the leucoemeraldine form of PANI [114]. The band at around 435 nm occurred in poly(**III**) can be assigned to radical cations which still exist even at -0.2 V [115]. As seen in both spectra, the absorption profile of these two type of intermediate are different. Relative absorption of radical cation of either poly(**III**) (Figure 3.17) or poly(**III**-co-ANI) (Figure3.29(b)) are lower than that of PANI intermediate. Besides the intensity growth of the band at around 860 nm in the spectra, there is a shift to lower wavelengths (blue shift) as the applied potential increases. This shows the oxidation of PANI from leucoemeraldine form to emeraldine form [114]. Similar behavior was also observed in poly(**III**-co-ANI) as well (Figure 3.29(b)). These shifts caused by the conformational changes during doping/dedoping (i.e. inclusion/exclusion of SO_4^{2-}) process for PANI [116] and poly(**III**-co-ANI). Such conformational changes described as compact coil or extended coil [117] can alter the absorption spectra.

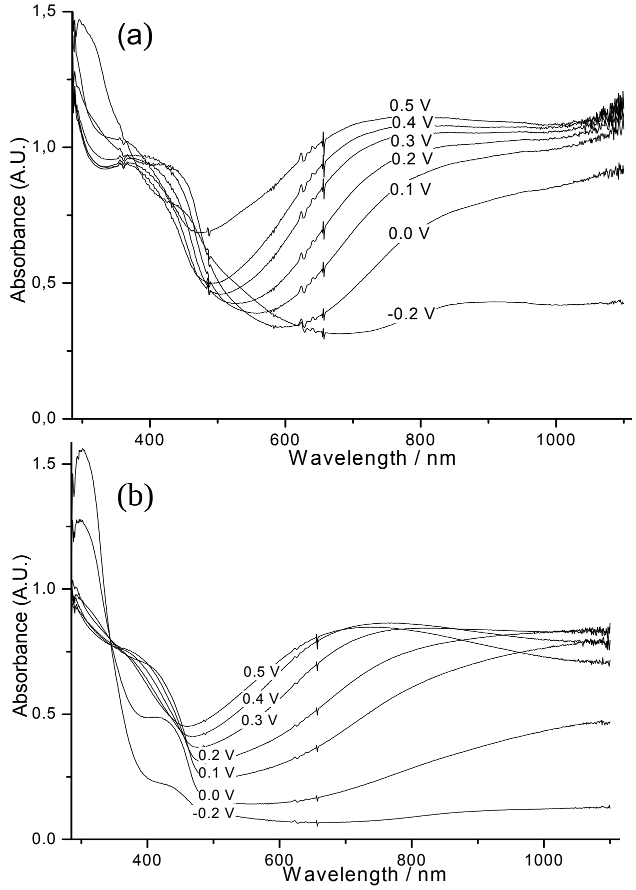

Figure 3.29 Electronic absorption spectra of (a) PANI (200 mC), (b) Poly(**III**-co-ANI) (200 mC) obtained from **MIII**/ANI mixture (2/10) in monomer-free aqueous solution of 3.0 M H_2SO_4.

Although there is no drastic changes between the electronic absorption spectra of PANI and poly(**III**-co-ANI) both in oxidized states, the E_g values show differences for both polymers (Figure 3.30).

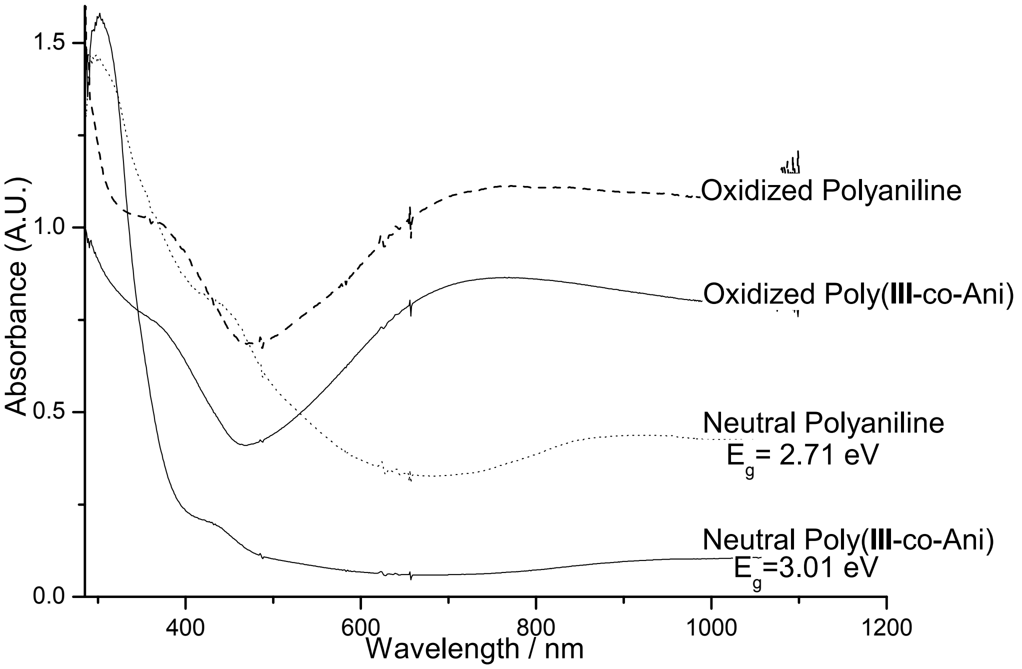

Figure 3.30 Comparison of electronic absorption spectra of the copolymer poly(**III**-co-ANI) and PANI in their neutral (-0.2 V vs. Ag-wire) and oxidized states (at +0.5 V vs. Ag-wire) 3.0 M H_2SO_4.

3.3.6 Temperature Dependent Conductivity of Copolymer

The temperature dependence of conductivity for the poly(**III**-co-ANI) and poly(**IV**-co-ANI) were investigated by applying constant current at various temperatures. Before changing the temperature, we have studied I-V behavior of the polymer film under vacuum. In the following figure the I-V behavior of poly(**III**-co-ANI), synthesized from 1/10:**MIII**/ANI mixture, can be seen. I-V measurements were done at 20 °C and -195 °C and the resistance values were calculated.

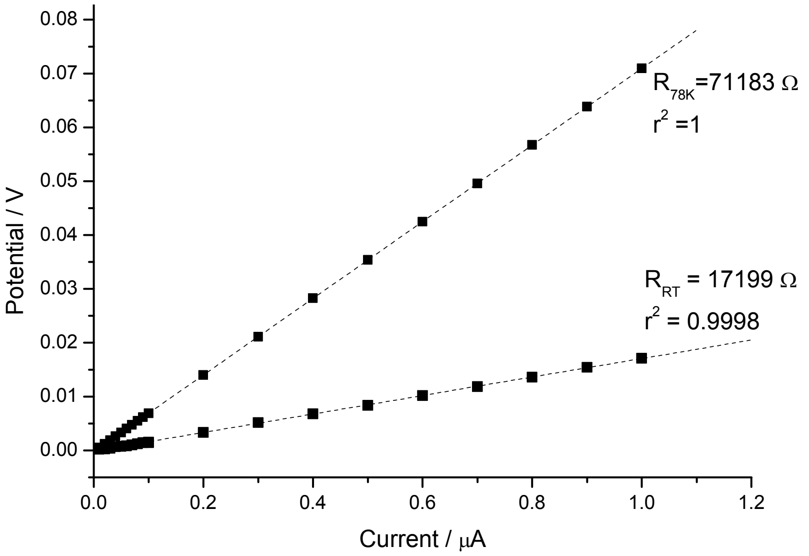

Figure 3.31 I-V behavior of poly(**III**-co-ANI) (from; **MIII**/ANI:1/10).

The temperature dependent conductivity was studied at a constant current which exists in the linear range of the above measurement done at minimum and maximum temperatures depicted in Figure 3.31 (i.e. 78 K and 295 K).

The temperature dependence of conductivity for the poly(**III**-co-ANI) and poly(**IV**-co-ANI) were analyzed according to following relation [47].

$$\sigma = \sigma_0 \exp\left(\frac{-E_a}{T}\right) \tag{3.1}$$

The conductivity-temperature profiles of the poly(**III**-co-ANI) and poly(**IV**-co-ANI) can be seen in Figure 3.32.

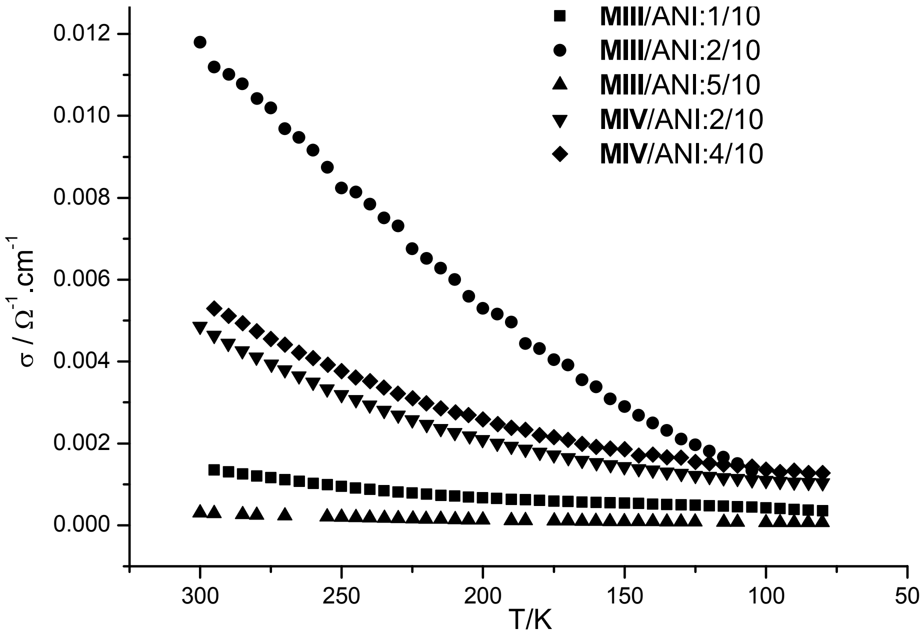

Figure 3.32 Temperature dependence of dc conductivity of poly(**III**-co-ANI) and poly(**IV**-co-ANI) with different compositions.

As seen from Figure 3.32, there are two linear regions below and above ~200 K. For poly(**III**-co-ANI), synthesized from a composition of **MIII**/ANI:2/10, the slopes of these regions gave activation energies of 25.5 and 39.6 meV for the temperatures lower and higher than 185 K, respectively. This result reveals that the ln(σ)-T^{-1} behavior is nonlinear, which is also valid for all copolymers in the given temperature interval. The nonlinear behaviors of two copolymers were shown in Figure 3.33.

The results were also analyzed according to Mott's variable range-hopping model (VRH) [47]. The expression for the temperature dependent conductivity is,

$$\sigma = \sigma_0 \exp\left(-\left(\frac{T_0}{T}\right)^{1/d+1}\right) \tag{3.2}$$

where d is dimensionality 1, 2, or 3.

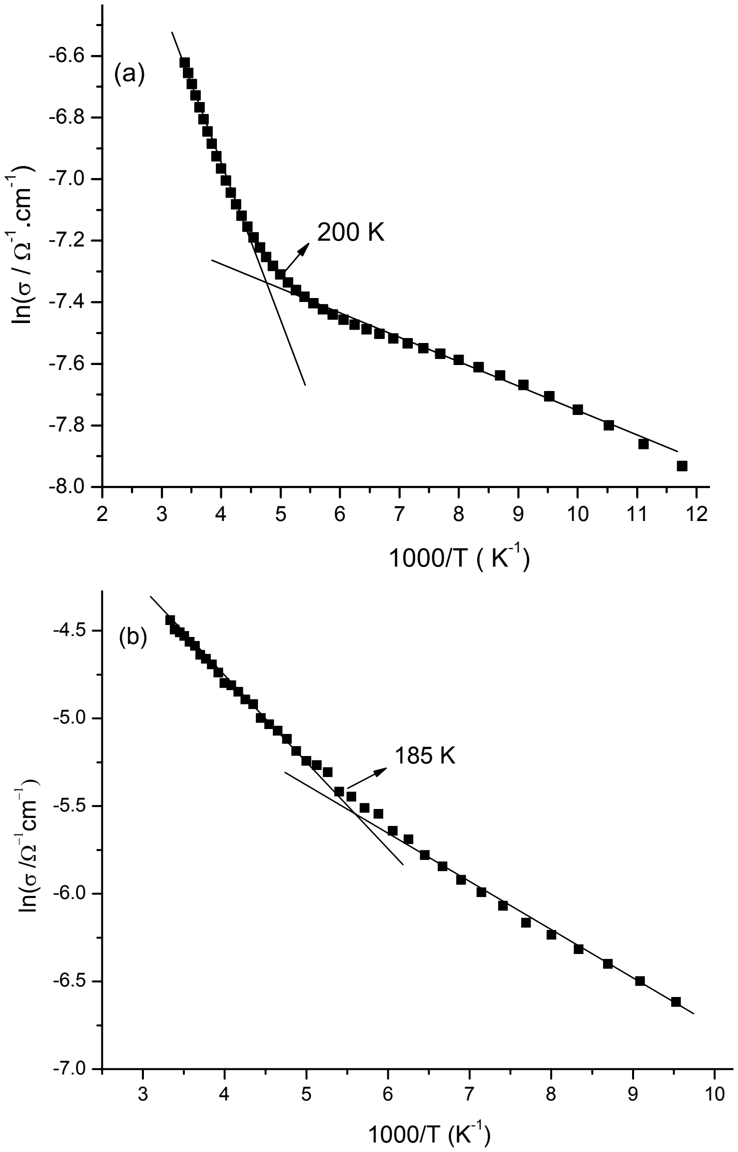

Figure 3.33 Temperature dependence of dc conductivity of poly(**III**-co-ANI);(a) **MIII**/ANI:1/10, (b) **MIII**/ANI:2/10.

In order to estimate the dimensionality of the hopping process we have obtained the plots of ln(σ) vs. $T^{-1/2}$, ln(σ) vs. $T^{-1/3}$, and ln(σ) vs. $T^{-1/4}$ (Figure 3.34 (a-c)). The small deviations from the linearity can be seen in the following figures which were drawn according to the equation (3.2).

Although all the plots depicted in Figure 3.34 seems to be linear, the most linear behavior for the temperature dependent conductivity of the poly(**III**-co-ANI) exists in three dimension revealed by the plot of ln(σ) vs. $T^{-1/4}$ with a regression coefficients of 0.9994 (Figure 3.34(c)).

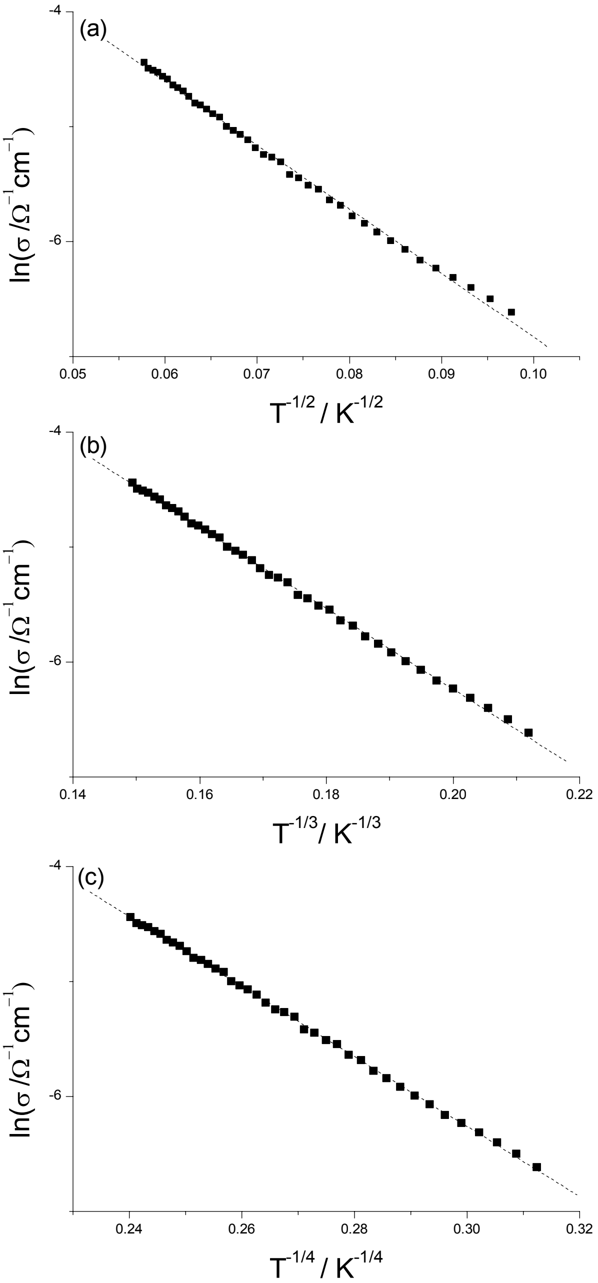

Figure 3.34 The dc conductivity changes of poly(**III**-co-ANI) as a function of (a) $T^{-1/2}$,(b) $T^{-1/3}$, (c) $T^{-1/4}$.

The temperature dependence of the effective density of states normalization was done by plotting ln(σ$T^{1/2}$) versus $T^{-1/4}$ (Figure 3.32) [118,119]. Although the plot is linear between 100-300 K the Mott's parameters were also calculated in order to check the Mott's requirements by using following equations:

$$\sigma\sqrt{T} = \sigma_0 \exp\left(-\left(\frac{T_0}{T}\right)^{1/d+1}\right) \tag{3.3}$$

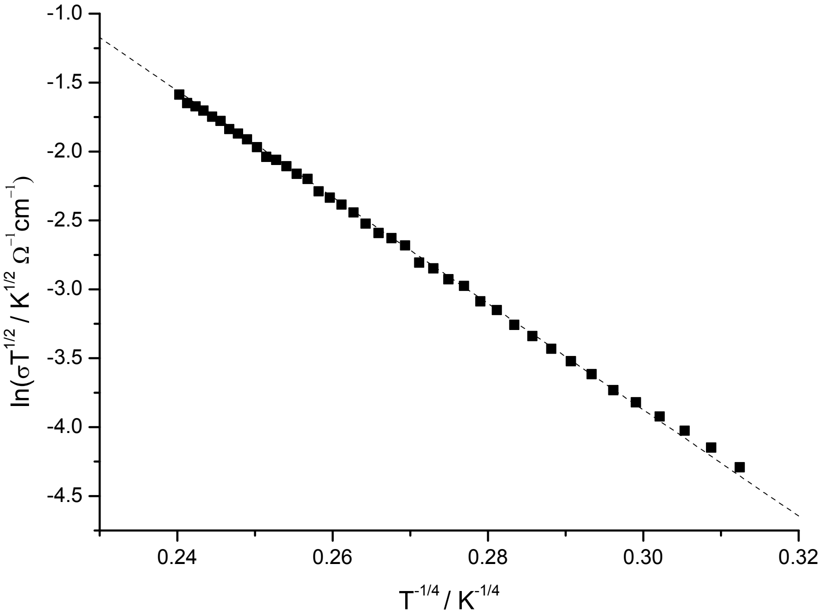

Figure 3.35 Plot of ln(σ$T^{1/2}$) as a function of $T^{-1/4}$ (r^2 = 0.999).

The following expressions were used for the determination of Mott's variables;

$$T_0 = \frac{\lambda\alpha^3}{k_B N(E_F)} \tag{3.4}$$

$$\sigma_0 = e^2 \upsilon R^2 N(E_F) \tag{3.5}$$

where σ_0 is the pre-exponential factor and T_0 is the characteristic temperature found from the intercept and slope of ln(σ$T^{1/2}$) versus $T^{-1/4}$, respectively. λ is the dimensionless constant (≈18.1), *e* is the electronic charge. α is the coefficient of exponential decay of the localized states and α^{-1} was assumed as 10Å [119], the characteristic phonon frequency υ is ≈10^{13} Hz [120,121], *k* is the Boltzmann's constant, and $N(E_F)$ is density of localized states at the Fermi level. The definition of the average hopping distance R and the average hopping energy W are as follows.

$$R = \{9/[8\pi\alpha k_B T N(E_F)]\}^{1/4} \tag{3.6}$$

$$W = 3/[4\pi R^3 N(E_F)] \tag{3.7}$$

The values of Mott's parameters are tabulated in Table 3.3.

Table 3.3 The VRH parameters and the experimental values for poly(**III**-co-ANI) and poly(**IV**-co-ANI).

	MIII-ANI			**MIV**-ANI	
Parameters	1/10	2/10	5/10	2/10	4/10
σ_{300} (Ω^{-1}.cm^{-1}) x10^{-3}	1.6	11.8	0.30	4.86	5.33
σ_0 (Ω^{-1}.cm^{-1}) x10^{2}	2.08	17.9	1.031	15.2x 10^3	74.9
T_0 (K) (x10^6)	2.05	2.04	2.93	2.80	1.97
λ	18.1	18.1	18.1	18.1	18.1
α (cm^{-1})	10^7	10^7	10^7	10^7	10^7
υ (Hz)	10^{13}	10^{13}	10^{13}	10^{13}	10^{13}
$N(E_F)$ (cm^{-3}.eV^{-1}) (x10^{19})	10.246	10.272	7.15764	7.49335	10.652
R(300K)(cm) (x10^{-8})	34.1	34.077	37.30	36.87	33.77
W(300K) (meV)	58.77	58.73	64.28	63.55	58.20

As mentioned above the VRH mechanism in three dimensions explains the conductivity of poly(**III**-co-ANI) between the temperatures of 100 – 300 K and the calculated parameters are consistent with Mott's requirements that αR>>1 and W>>kT.

3.4 Calibration of Modified GCE for Cation Analysis by Differential Pulse Anodic Pulse

3.4.1 Preparation of Poly(III) Modified GCE

Since poly(**III**) and poly(**IV**) possibly would contain cavities (see Figure 3.14) into which various cations can be localized, we have also investigated their affinities towards various cations. For this purpose, a 1.6 mm diameter glassy carbon electrode, GCE, was modified by coating its surface with a thin film of poly(III). Polymerization was achieved in 3.0 M H_2SO_4 solution by applying repetitive cycles between 0 and 1.0 V vs. Ag/AgCl. Since the film thickness is an important parameter, we have optimized the film thickness by synthesizing the polymer film on GCE via ten successive cycles. After coating with polymer the electrode was washed with acid solution to remove any monomer and then rinsed with deionized water.

3.4.2 Stripping Voltammetry Medium

There are many choices for electrolytic medium such as HNO_3 [122], Na_2HPO_4 [123], HNO_3-NH_4OH [124], $NaNO_3$ [125], $NaOOCH_3$-CH_3COOH [126,127,128,129,130,131,132], NH_3-NH_4Cl [133], and Britton-Robinson [134] buffer solutions, etc. depending on the metals to be analyzed and the type of the polymer film to investigate the voltammetric behavior of the modified electrode. In this study, since poly(**III**) is electroactive in acidic solution, stock solutions were prepared in 0.01 M HNO_3. It was observed that no signal could be observed in the absence of acids [135] and also no peaks were detected at pH lower than 4 [136]. Therefore, a moderately acidic buffer solution of CH_3OONa and CH_3COOH was chosen for this study. The pH of solution was about 4.5 - 5.0.

3.4.3 Effect of Stripping Parameters

Accumulation potential, accumulation time, pulse size, pulse time, sample period are the examples of important parameters for stripping analysis.

As the accumulation potential increased to greater potential values (in negative sense) the anodic striping peak current of metal oxidation increased. However, one must be careful in choosing the accumulation potential because more negative values causes undesired metal ions or H^+ ions to be reduced. The reduction of such ions definitely will cause interfering currents which affects the desired anodic peak current. Therefore, the optimized accumulation potential in this system was chosen as -1.2 V.

Other conditions of anodic stripping experiments are the pulse time, pulse height, step size, and the sample period. In order to have narrower and higher signals during the ASV experiments, following stripping parameters were chosen: Pulse height=25 mV, pulse time= 20 ms, step size=5 mV, and sample period=2 s.

3.4.4 General Procedure for Stripping Voltammetry

In order to start analysis, the stock solutions were prepared in 0.01 M HNO_3 and 20 μL of these solutions were added sequentially before each stripping procedure. Before the stripping, solutions were stirred and accumulation potential of -1.2 V was applied during 120 s and let to settle for 30 s. The optimized stripping parameters were used throughout the analysis of three metals.

3.4.5 Calibration for Analysis of Pb^{2+}, Cd^{2+}, and Cu^{2+} by Differential Pulse Anodic Stripping Voltammetry

The stripping analysis of Pb^{2+} ion was done and the voltammogram was given in Figure 3.36. The oxidation potential of Pb metal was about -0.5 V and as the concentration increased the oxidation potential shifted towards positive direction slightly (about 40 mV).

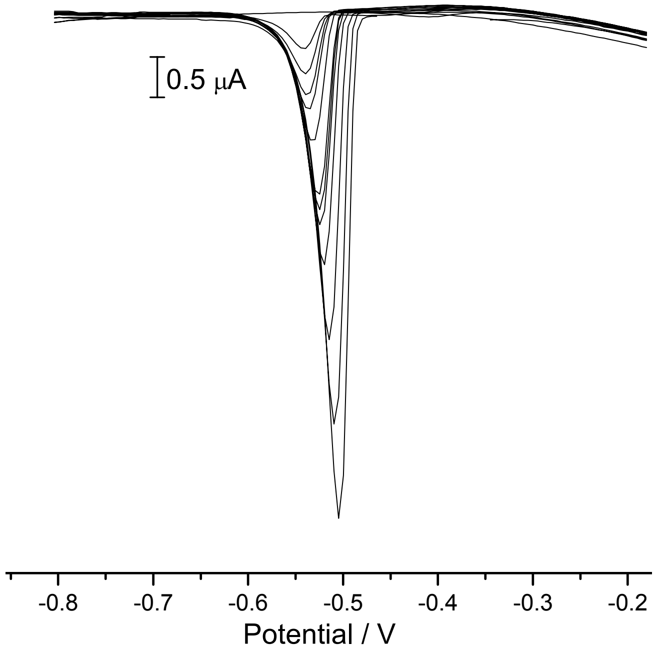

Figure 3.36 DPSV voltammograms of Pb^{2+} at pH of 4.6 with a pulse height of 25 mV, a pulse time of 20 ms, a step size of 5 mV, and the sample period of 0.2 s.

The stripping analysis of Cd^{2+} and Cu^{2+} ions were also investigated utilizing the poly(**III**) modified GCE under the same experimental conditions. The calibration plots were obtained according to stripping current of oxidized metal and the reproducibility was checked with four measurements for each concentration (Figure 3.37 a-c). The calibration plot showed good linearity between 1.2 – 8.4 ppm values for Cd^{2+} and between 1-9.0 ppm for Cu^{2+}.

Although the calibration plots have good linearity for the modified GCE, the detection limits were not as good as bare GCE. Therefore, no further studies were done for cation sensing.

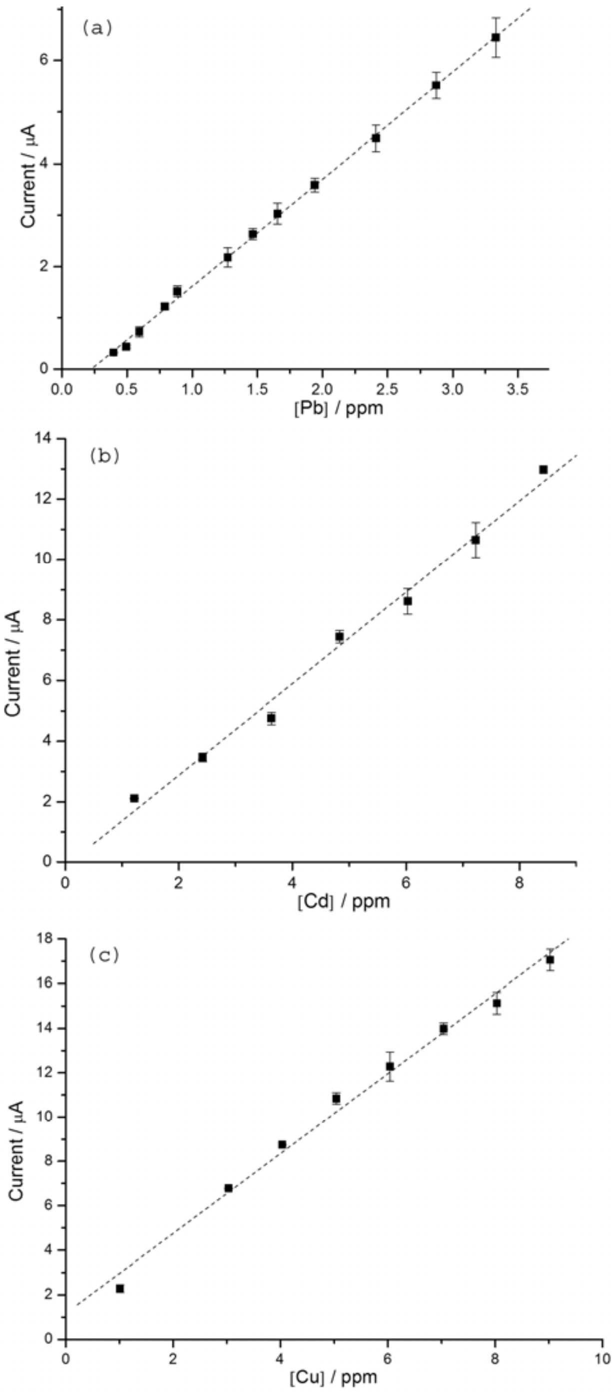

Figure 3.37 Calibration plots of poly(III) modified GCE for (a) Pb^{2+} ($r^2 = 0.999$), (b) Cd^{2+} ($r^2 = 0.990$), and (c) Cu^{2+} ($r^2 = 0.991$) at pH of 4.6 with a pulse height of 25 mV, a pulse time of 20 ms, a step size of 5 mV, and the sample period of 0.2 s.

CHAPTER 4

CONCLUSIONS

In this work four different polyether substituted Th and ANI derivatives were synthesized and characterized by ^{1}H-NMR, ^{13}C-NMR, FTIR.

Electrochemical polymerization of **MI** and **MII** in TBAPF6/CH_3CN electrolytic medium yielded bright black free standing films. Although, both poly(**I**) and poly(**II**) exhibit reversible redox behavior in the monomer-free environment indicating reversible doping/de-doping of the polymer films they were found to have low electrical conductivities which can be enhanced via chemical doping. In-situ ESR studies indicated that this enhancement is not permanent and chemically doped poly(**I**) and poly(**II**) experiences a drastic decrease in conductivity. This is also confirmed by in-situ UV-vis measurements and can be attributed to higher sensitivity of the polymer film to moisture because of the presence of the polyether spacer in the polymer backbone. Thus, poly(**I**) and poly(**II**) films are more stable in the neutral state than in the oxidized state.

On the other hand, free-standing polymer films from **MIII** and **MIV** were only possible in aqueous solution with high acid concentration (i.e. 3.0 mol.L^{-1} H_2SO_4). The FT-IR spectroscopy was used to estimate that whether the polyether bridges were broken during the polymerization process or not. The inspection of the FT-IR spectra of poly(**III**) and poly(**IV**) revealed that polyether bridges still exist in polymers.

The spectroelectrochemical behaviors of the polymers were also studied in order to have information on band gap, maximum absorption wavelengths, and polaron–bipolaron formations upon doping process. For these purposes UV-vis spectroscopy was used. The E_g values of poly(**I**) and poly(**II**) were found to be greater than the one for PTh. In addition to this, the E_g values of poly(**III**) and poly(**IV**) were higher than that of PANI as well.

The conductivities of the polyether bridged Ths, poly(**I**) and poly(**II**), were vanishing which might be attributed to sensitivity of the polymer films to the moisture. The conductivities of the poly(**III**) and poly(**IV**) were also found to be very low and this can be attributed to the decreasing conjugation length.

In order to increase the conductivities of poly(**III**) and poly(**IV**) the copolymerization with aniline were tried. The electrochemical and spectroelectrochemical behaviors were studied and the copolymerization was verified. The FTIR spectroscopy was used to confirm the presence of polyether chains in polymer backbones. The reasonable conductivities were achieved for the copolymers obtained from all compositions.

The conduction mechanisms for the polymers obtained in the form of free standing films were studied and it was found that the conduction mechanisms of the polymer films obey the Mott's variable range hopping process in three dimensions within given temperature intervals.

Since, poly(**III**) and poly(**IV**) possibly contains pseudo-polyether cages in the polymer backbone, they were investigated in terms of cation sensing properties. This was achieved on a modified GCE. The calibration plots were obtained for Pb^{2+}, Cd^{2+}, and Cu^{2+} and it was observed that the detection limit was not as good as that of bare glassy carbon electrode itself. Therefore, no further investigations as to cation sense were done.

REFERENCES

1 - C.K. Chiang, C.R Fincher, Y.W. Park, A.J. Heeger, H .Shirakawa, F.J. Louis, S.C. Gau, A.G. MacDiarmid, Phys. Rev. Lett., 1977, 39, 1098.

2 - A. F. Diaz, K. K. Kanazawa, G. P. Gardini, J. Chem. Soc., Chem. Commun., 1979, 14, 635.

3 - A. F. Diaz, J. I. Castillo, J. A. Logan, W. Lee, J. Electroanal. Chem., 1981, 129, 115.

4 - K. Lee, A. J. Heeger, Synth. Met., 1997, 715.

5 - A. F. Diaz, Chem. Scr.,1981, 17, 142.

6 - G. Tourillon, F. J. Garnier, J. Electroanal. Chem., 1982, 135, 173.

7 - Bayer AG Eur. Patent., 1988, 339, 340.

8 - F. Jonas, L. Schrader, Synth.Met., 1991, 41-43, 831.

9 - G. Heywang, F. Jonas, Adv. Mater., 1992, 4, 116.

10 - A. Gandini, M. N. Belgancem, Prog. Polym. Sci., 1997, 22 1203.

11 - A. Desbene-Monvernay, P.-C. Lacaze, J.-E. Dubois, J. Electroanal. Chem., 1981, 129, 229.

12 - J. Rault-Berthelot, J. Simonet, J. Electrochem. Soc., 1985, 182 187.

13 - A. G. MacDiarmid, A. Epstein, J. Farad. Discuss. Chem. Soc., 1989, 88 317.

14 - J. H. Burroughes, D. D. C. Bradley, A. R. Brown, R. N. Marks, K. MacKay, R. H. Friend, P. L. Burn, A. B. Holmes, Nature , 1990, 347, 539.

15 - G. Grem, G. Leditzky, B. Ullrich, G. Leising, Adv. Mater., 1992, 4, 36.

16 - K.Doblhofer, K.Rajeshwar, Handbook of Conducting Polymers. T.A. Skotheim, R.A .Elsenbaumer, J.R. Reynolds, New York: Marcel Dekker, 1998.

17 - J. H. Burroughes, C. A. Jones, R. H. Friend, Nature 1988, .335, 137.

18 - G.G. Wallace, M. Smyth, H. Zhao, Trends in Analytical Chemistry, 1999, 18, 245.

19 - A. Moliton, C. R. Hiorns, Polym. Int. 2004, 53, 1397.

20 - A. Cravino, N. S. Sariciftci, J. Mater. Chem., 2002, 12, 1931

21 - S. Asavapiriyonont, G. K. Chandler, G. A. Gunawardena, D. J. Pletcher, J. Electroanal. Chem., 1984, 177, 229.

22 - T. Inoue, T. Yamase, Bull. Chem. Soc. Jpn.,1983, 56, 985.
23 - E. Genies, G. Bidan, A. F. Diaz, J. Electroanal. Chem.,1983, 149, 113.
24 - R. J. Waltman, J. Bargon, Tetrahedron, 1984, 40, 3963.
25 - T. Okada, T. Ogata, M. Ueda, Macromolecules, 1996, 40, 3963.
26 - K. Yoshino, R. Hayashi, R. Sugimoto, J. Appl. Phys., 1984, 23, L899.
27 - M. Pomerantz, J.J. Tseng, H. Zhu, S.J. Sproull, J.R. Reynolds, R. Uitz, H.J. Arnott, Synth. Met.,1991, 41-43, 825.
28 - N. Toshima, S. Hara, Prog. Polym. Sci., 1995, 20, 155
29 - R.H. Baughman, J.L. Brédas, R.R. Chance, R.L. Elsenbaumer, L.W. Shacklette, Chem. Rev., 1982, 82, 209.
30 - B.G. Street, T.C. Clarke, M. Krounbi, K. Kanazawa, V. Lee, P. Pfluger, J.C. Scott, G. Weiser, Mol. Cryst. Liq. Cryst.,1982, 83, 1285.
31 - T. Shimidzu, A. Ohtani, T. Iyoda, K.J. Honda, J. Chem. Soc., Chem. Commun., 1982, 361.
32 - J.I. Reddinger, J.R. Reynolds, Advances in Polymer Science, 1999, 45, 59.
33 - J.C.W. Chien, Polyacetylene: Chemistry, Physics, and Material Science; Academic Press, Inc.: Orlando, 1984.
34 - U. Salzner, J. B. Lagowski, P.G. Pickup, R.A. Poirier, Synth. Met., 1998, 96, 177.
35 - J. L. Bredas, B. Themans, J. G. Fripiat, J. M. Andre, R. R. Chance, R. R. Phys. Rev. B:Condens. Matter., 1984, 29, 6761.
36 - J.L. Bredas, G.B. Street, Acc. Chem. Res., 1985, 18, 309.
37 - K. Fesser, A.R. Bishop, D.K. Campbell, Phys. Rev., 1983, B 27, 4804.
38 - H. Shirakawa, E.J. Louis, A.G. Macdiarmid, C.K. Chiang, A. J. Heeger, J. Chem. Soc.-Chem. Commun., 1977, 578.
39 - W.R. Salaneck, I. Lundstrom, W.S. Huang, A.G. Macdiarmid, Synth. Met., 1986, 13, 291.
40 - P.J. Nigrey, A.G. Macdiarmid, A.J. Heeger, J. Chem. Soc.-Chem. Commun., 1979, 594.
41 - A.F. Diaz, J. Bargon, In Handbook of Conducting Polymers; Vol. 1; Skotheim, T.A.; Ed.; Marcel Dekker: New York, 1986, 82.
42 - L. van der Pauw, J. Philips Technical Review, 1958, 20, 220.
43 - A.R. Blythe, Polymer Testing, 1984, 4, 195.
44 - J Smits, F. M. Bell System Technical Journal, 1958, 37, 711.

45 - I. Schwendeman, PhD Thesis, University of Florida, 2002.

46 - L. B. Valdes, Proceedings of the Institute of Radio Engineers, 1954, 42, 420.

47 - N.F. Mott and E.A. Davis, Electronic Processes in Non-Crystalline Materials, Clarendon Press, Oxford, 1971.

48 - D. Schäfer-Siebert, S. Roth, Limitation of the Conductivity of the Polyacetylene by Conjugation Defects, paper presentation at ICSM'88, Santa Fe, California, USA, 1988.

49 - J.J., Hauser, J. Non-Cryst. Solids, 1977, 23, 21.

50 - R. Singh, A.K. Narula, R.P. Tandon, A. Mansingh, S. Chandra, J. Appl. Phys., 1997, 81, 3726.

51 - P. Sheng, Phys. Rev. B, 1980, 21, 2180.

52 - S. Kivelson, Phys. Rev., B, 1982, 21, 3798.

53 - S. Kivelson, A.J. Heeger , Pys. Rev. Lett., 1985, 55, 308.

54 - J.M. Pernaut, J. R. Reynolds, J. Phys. Chem. B., 2000, 104, 4080.

55 - P.M.S. Monk, R.J. Mortimer, D.R. Rosseinsky, Electrochromism: Fundamentals and Applications; VCH: Weinheim, 1995.

56 - J.C. DuBois, O. Sagnes, F. Henry, Synth. Met., 1989, 28, C871.

57 - P. Novak, K. Muller, K.S.V. Santhanam, O. Haas, Chem. Rev., 1997, 97, 207.

58 - T.A. Skotheim, R.L. Elsenbaumer, J.R. Reynolds, Eds. Marcel Dekker: New York, 1998.

59 - D.T. McQuade, A.E. Pullen, T.M. Swager, Chem. Rev., 2000, 100, 2537.

60 - J.M. Pernaut, J.R. Reynolds, J. Phys. Chem. B., 2000, 104, 4080.

61 - C.J. Pedersen, J. Am. Chem. Soc., 1967, 89, 7017.

62 - C.J. Pedersen, Angew. Chem., Int. Ed. Engl., 1988, 27, 1021.

63 - J.J. Christensen, J.O. Hill, R.M. Izatt, Science, 1971, 174, 459.

64 - J.J. Christensen, D.J. Eatough, R.M. Izatt, Chem. Rev., 1974, 74, 351.

65 - N.S. Poonia, A.V. Bajaj, Chem. Rev., 1979, 79, 389.

66 - I.M. Kolthoff, Anal. Chem., 1979, 51, 1R.

67 - M. Takagi, H. Nakamura, J. Coord. Chem., 1986, 15, 53.

68 - C.J. Pedersen, H.K. Frensdorff, Angew. Chem., Int. Ed. Engl., 1972, 11, 16.

69 - C.J. Pedersen, J. Am. Chem. Soc., 1970, 92, 386.

70 - V. Le Berre, L. Angely, N. Simonet-Gueguen, J. Simonet, New J. Chem., 1985, 9, 419.

71 - V. Le Berre, L.Angely, N. Simonet-Gueguen, J. Simonet, J. Electroanal. Chem., 1986, 206, 115.

72 - A. Cihaner, A.M. Önal, J.Electroanal. Chem., 2004, 571, 159.

73 - J. Roncali, Chem. Rev., 1992, 92, 711.

74 - M. Lemaire, R. Garreau, J. Roncali, D. Delabouglise, H. Korri-Youssoufi, F. Garnier, New J. Chem., 1989, 13, 863.

75 - J. Roncali, R. Garreau, D. Delabouglise, F. Garnier, M. Lemaire, J. Chem. Soc., Chem. Commun., 1989, 679.

76 - J. Roncali, R. Garreau, M. Lemaire, J. Electroanal. Chem., 1990, 278, 373.

77 - J.M. Barker, J.D.E. ChaYn, J. Halfpenny, P.R. Huddleston, P.F. Tseki, J. Chem. Soc., Chem. Commun., 1993 1733.

78 - P. Marrec, B. Fabre, J. Simonet, J. Electroanal. Chem., 1997, 437, 245.

79 - R. A. Robinson, R. H. Stokes, Electrolyte Solutions, Butterworths Scientific Publications, London , 1959.

80 - S. Tirkeş, A. Cihaner, A.M. Önal, J. Electroanal. Chem., 2004, 573, 189.

81 - P. Marrec, J. Simonet, J. Electroanal. Chem., 1998, 459, 35.

82 - A. Kitani, H. Munemura, K. Takaki, and S. Ito, Synth. Met., 1997, 84, 101.

83 - A. Kitani, H. Munemura , T. Yamashita, and Ito S, Synth. Met., 1999, 102, 1173.

84 - S. Tirkeş, A. Cihaner, A.M. Önal, Polym. Int., 2007, 56, 1040.

85 - A. Bard, L.R. Faulkner, Electrochemical Methods: Fundamentals and Applications; John Wiley & Sons: New York, NY, 1980.

86 - J. Wang, Stripping Analysis: Principles, Instrumentation and Applications, VCH Publishers, Deerfield Beach, FL, 1985.

87 - T.R. Copeland, R.K. Skogerboe, Anal. Chem.1974, 46, 1257A.

88 - C.H. Goeting, F. Jones, J.S. Foord, J.C. Eklund, F. Marken, R.G. Compton, P.R. Chalker, C.J. Johnston, C. J. Electroanal. Chem 1998, 442, 207.

89 - M. Awada, J.W. Strojek, G.M. Swain, J. Electrochem. Soc. 1995, 142, L42.

90 - C. Prado, S.J. Wilkins, F. Marken, R.G. Compton, Electroanal. 2002, 14, 262.

91 - N. Vinokur, B. Miller, Y. Avyigal, R.J. Kalish, Electrochem. Soc. 1999, 146, 125.

92 - E. Sahlin, D. Jagner, R.R. Ratana-ohpas, Anal. Chim. Acta. 1997, 346, 157.

93 - J. Wang, B. Tian, Anal. Chem., 1993, 65, 1529.

94 - X.H. Zhang, S.F. Wang, Sens. Actuators B: Chem., 2005, 104, 29.

95 - M. Brand, I. Eshkenazi, E. Kirowa-Eisner, Anal. Chem., 1997, 69, 4660.

96 - B. Krasnodebska-Ostrega, J. Piekarska, Electroanalysis, 2005, 17, 815.

97 - K. Wu, S. Hu, J. Fei, W. Bai, Anal. Chim. Acta, 2003, 489, 215.

98 - J. Di, F. Zhang, Talanta, 2003, 60, 31.

99 - P. Calvo-Marzal, K.Y. Chumbimuni-Torrs, N.F. Hoehr, G.O. Neto, L.T. Kubota, Sens. Actuators B: Chem., 2004, 100, 333.

100 - G. Roa-Morales, M.T. Ramirez-Silva, R.L. Gonz´alez, L. Galicia, M. Romero-romo, Electroanalysis,2005, 17, 694.

101 - C. Hu, K. Wu, X. Dai, S. Hu, Talanta, 2003, 60, 17.

102 - J.B. He, C.L. Chen, J.H. Liu, Sens. Actuators B: Chem., 2004, 99, 1.

103 - K.C. Honeychurch, J.P. Hart, D.C. Cowell, D.W.M. Arrigan, Sens. Actuators B: Chem., 2001, 77, 642.

104 - K.C. Honeychurch, J.P. Hart, D.C. Cowell, D.W.M. Arrigan, Electroanalysis, 2002, 14, 177.

105 - P. Marrec, B. Fabre, J. Simonet, J. Electroanal. Chem., 1997, 437, 245.

106 - A.A. Ibrahim, M. Matsumoto,Y. Miyahara, K. Izumi, M. Suenaga, N. Shimizu, et al, J. Heterocycl. Chem., 1998, 35, 209.

107 - F.A. Viva, E.M. Andrade, F.V. Molina, and M.I. Florit, J. Electroanal. Chem., 1999, 471, 180.

108 - T.Lindfors, A. Ivaska, J. Electroanal. Chem, 2002, 531, 43.

109 - C. Barbero, M.C. Miras, O. Haas, R. Kötz, J. Electroanal. Chem, 1991, 310, 437.

110 - Y. Wei, W.W. Focke, G.E. Wnek, A. Ray, A.G. MacDiarmid, J. Phs. Chem., 1989, 93, 495.

111 - S.I. Córdoba de Torresi, A.N. Bassetto, B.C. Trasferetti, J. Solid State Electrochem., 1998, 2, 24.

112 - H. S. Nalwa, Handbook of Organic Conductive Molecules and Polymers: vol. 2 Conductive Polymers: Synthesis and Electrical Properties, John Wiley & Sons ltd., 1997.

113 - A.A. Shah, R. Holze, Synth. Met, 156, 2006, 566.

114 - A.A. Shah, R. Holze, Electrochimica Acta, 2006, 52, 1374.

115 - S. Shreepathi, R. Holze, Chem. Mater. 2005, 17, 4078.

116 - A.J. Dominis, G.M. Spinks, L.A.P. Kane-Maguire, G.G. Wallace, Synth. Metal., 2002, 129, 156.

117 - Y. Min, Y. Xia, A.G. MacDiarmid, A.J. Epstein, Synth. Metal., 1995, 69, 159.

118 - M. Ghosh, A. Barman, A.K. Meikap, S.K. De, S. Chatterjee, Phys. Lett. A., 1999, 260, 138.

119 - A. Sarkar, P. Ghosh, A.K. Meikap, S.K. Chattopadhyay, S.K. Chatterjee, M. Ghosh, Solid State Commun., 2007, 143, 358.

120 - D.K. Paul, S.S. Mitra, Phys. Rev. Lett., 1973, 31, 1000.

121 - A. Bozkurt, M. Parlak, Ç. Erçelebi, L. Toppare, J. Appl. Polym. Sci., 2002, 85, 52.

122 - C. Parat, S. Betelu, L. Authier, M.P. Gautier, 2006, 14, 573.

123 - C. Hu, K. Wu, X. Dai, S.Hu, Talanta 2003, 60, 17.

124 - C. Bing, R. Deen, G.N. Khang, C.L. Sai, L. Kryger, Talanta, 1999, 49, 651.

125 - S. Noel, M.L.T Waeber, L. Lin, J. Buffle, O. Guenat, M.K. Hep, Electroanalysis, 2006, 21, 2061.

126 - A. Wanekaya, O.A. Sadik, J. Eletroanal. Chem., 2002, 537, 135.

127 - D. Sancho, M. Vega, L. Deban, R. Pardo, G. Gonzalez, Analyst, 1997, 122, 727.

128 - A.N. Onar, A. Temizel, Analyst, 1987, 112, 227.

129 - A. Manivannan, R. Kawasaki, D.A. Tryk, A. Fujishima, Electrochim. Acta., 2004, 29, 3313.

130 - S.B. Khoo, J. Zhu, Anal. Chim. Acta, 1998, 373, 15.

131 - B.S. Sherigara, Y Shivaraj, R.J. Mascarenhas, A.K. Satpati, Electrochim. Acta, 2007, 52, 3137.

132 - S.B.Hocevar, I. Svancara, K. Vytras, B. Ogorevc, Electrochim. Acta, 2005, 51, 706.

133 - J. Wang, J. Lu, Electrochem. Comm., 2000, 2, 390.

134 - O.E.Hernandez, I.N. Rodriguez, J.L.H.H. Cisneros, E. Reguera, Sensors and Actuators B, 2006, 123, 488.

135 - Y. Bonfil, M. Brand, E.K. Eisner, Anal. Chim. Acta, 2002, 464, 99.

136 - J.V. van Staden, M.C. Matoetoe, Anal. Chim. Acta, 2000, 411, 201.

CURRICULUM VITAE

PERSONAL INFORMATION

Surname, Name: Tirkeş, Seha
Nationality: Turkish (T.C.)
Date and Place of Birth: 26 June 1977, Ankara
Marital Status: Single
Phone: +90 312 241 01 69
Fax: +90 312 586 80 91
E-mail: stirkes@atilim.edu.tr

EDUCATION

Degree	**Institution**	**Year of Graduation**
MS	METU Chemistry Department	2001
BS	METU Chemistry Department	1999
High School	Antalya High School, Antalya	1994

WORK EXPERIENCE

Year	**Place**	**Enrollment**
2004-	Atılım University	Instructor
2001-2004	Atılım University	Research Assistant
1998 July	Hoechst Marion Roussel Quality Control Lab	Intern Research Student

FOREIGN LANGUAGES

Advanced English

PUBLICATIONS

1. S.Tirkeş, L.Toppare, S.Alkan, U.Bakır, A.Önen, Y.Yağcı ‘Immobilization of glucose oxidase in polypyrrole / polytetrahydrofuran graft copolymers’ International Journal of Biological Macromolecules 30, (2002), 81
2. S. Tirkeş, A. Cihaner, A. M. Önal ‘Electrochemical Polymerization of 9-Fluorenone’ J. Electroanal Chem, Journal of Electroanalytical Chemistry, 568, (2004), 151.
3. S. Tirkeş, A. Cihaner, A. M. Önal, ‘Synthesis and polymerization of 2- and 3-substituted thiophene derivatives linked by polyether bridges’, Journal of Electroanalytical Chemistry, 573, (2004), 1, 189.
4. S. Tirkeş, A. Cihaner, A. M. Önal, ‘Electrochemical polymerization and characterization of polyether-substituted aniline derivatives’, Polymer International, 56, 8, (2007), 1040.
5. S. Tirkeş, A. M. Önal, ‘Electrosynthesis of polyfuran in acetonitrile-boron trifluoride-ethyl ether mixture and its device application’ Journal of Applied Polymer Science, 103, 2, (2007), 871.

HOBBIES

Swimming, sailing